

# Reduced models for flow in porous media containing faults with discretization using hybrid finite volume schemes

Isabelle Faille, Alessio Fumagalli, Jérôme Jaffré, Jean Roberts

▶ **To cite this version:**

Isabelle Faille, Alessio Fumagalli, Jérôme Jaffré, Jean Roberts. Reduced models for flow in porous media containing faults with discretization using hybrid finite volume schemes. 2015. hal-01162048

**HAL Id: hal-01162048**
**https://ifp.hal.science/hal-01162048**

Preprint submitted on 9 Jun 2015

**HAL** is a multi-disciplinary open access archive for the deposit and dissemination of scientific research documents, whether they are published or not. The documents may come from teaching and research institutions in France or abroad, or from public or private research centers.

L'archive ouverte pluridisciplinaire **HAL**, est destinée au dépôt et à la diffusion de documents scientifiques de niveau recherche, publiés ou non, émanant des établissements d'enseignement et de recherche français ou étrangers, des laboratoires publics ou privés.

# Reduced models for flow in porous media containing faults with discretization using hybrid finite volume schemes

Isabelle Faille [*1], Alessio Fumagalli [†1], Jérôme Jaffré [‡2], and Jean E. Roberts [§2]

[1]IFP Energies nouvelles, 1 & 4 avenue de Bois-Préau 92852 Rueil-Malmaison Cadex - France
[2]INRIA Roquencourt, BP 105, 78153 Le Chesnay Cadex - France

## Abstract

In this paper we study two different model reduction strategies for solving problems involving single phase flow in a porous medium containing faults or fractures whose location and properties are known. These faults are represented as interfaces of dimension $N-1$ immersed in an $N$ dimensional domain. Both approaches can handle various configurations of position and permeability of the faults, and one can handle discretization grids that do not match up at the fault interface. For the numerical discretization we use the hybrid finite volume scheme as it is known to be well suited to simulating subsurface flow. Some results, which may be of use in the implementation of the proposed methods in industrial codes, are demonstrated.

**Keywords:** Porous media, Faults, Interface model, Non-matching grids, Finite volumes

## 1 Introduction

Fluid flow in porous media can be strongly influenced by the presence of large faults, which, depending on their porosity and permeability, may act as preferential paths for flow linking geologically otherwise unconnected layers or as barriers isolating some part of the fluid. The faults may connect different parts of the domain and they may also intersect one another. Among the many domains of application requiring an accurate description of fluid flow in faulted media, we mention $CO_2$ injection and sequestration, oil migration and recovery, and prevention of groundwater contamination from underground nuclear waste disposal, to cite just a few.

Since the width of a fault is several orders of magnitude smaller than any other characteristic size of the porous medium in which it lies and since it is usually very small in comparison to the typical mesh size, it is unreasonable and often for real cases completely unaffordable to uniformly refine the computational grid to a degree that the fault may be represented exactly. To deal with this difficulty we consider approximation based on a reduced model (RM) in which flow along and across the fracture is described using a simplified set of equations. A reduced model for Darcy flow was introduced in [3] and extended in [17, 32]. In these references the authors propose a reduced model in which each fault is represented by a single $(N-1)$ dimensional object and flow in the fault is coupled with flow in the rest of the domain by suitable interface conditions. In this article we will refer to such a model as a *single layer-reduced model* (SLRM) or simply (SL). In the aforementioned works it was essentially supposed that the fault crossed the entire domain, so, to take into account fractures ter-

[*]isabelle.faille@ifpen.fr
[†]alessio.fumagalli1984@gmail.com
[‡]jerome.jaffre@inria.fr
[§]jean.roberts@inria.fr

minating in the interior of the domain, in [4], the authors extended the model by imposing no flow conditions on the tips of the faults lying in the interior of the domain. These models were all concerned with single phase Darcy flow. Other results considering similar single-layer reduced models for single phase Darcy flow include [5, 30, 29, 25, 26, 24, 27, 34, 35, 9] to name a few.

The SLRM has also been extended to treat nonlinear problems: in [21, 31] an extension was given that couples Forchheimer flow in the fracture with Darcy flow in the surrounding rock matrix. In [28] the authors extended the reduced model to treat a two-phase flow problem by introducing new non-linear coupling conditions for the saturation, which involve the capillary pressure, at the fault interface. Other authors have also treated the case of two-phase flow; we cite [37, 22, 33, 10] among others.

For information concerning other types of models for flow in porous media with faults and fractures, we simply cite some of the main references in the literature [7, 1, 8, 2].

For the numerical discretisation of these reduced models both finite element and finite volume methods have been analysed and used effectively showing the flexibility of the models with respect to discretisation method. In [20] it was shown that for the numerical discretization of the SLRM, the mesh on one side of the fracture does not need to match up with that on the other nor with the mesh inside the interface fracture. In [12, 23, 19] the authors went further and showed that by using extended finite elements the mesh on the rock matrix can be chosen completely independently of the fracture, allowing the fracture to cut across cells of the grid.

One application that particularly concerns us here is the simulation of sedimentary basins. In such basins, due to subsurface movements on a geological time scale, the surrounding porous medium on one side of a fault may slip with respect to that on the other. An example is depicted in Figure 1, where the right side of the domain has slipped with respect to the left side.

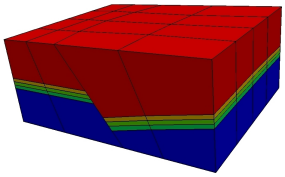


Figure 1: Example of a schematic basin with slippage along a fault.

To better deal with the case of slipping faults, in [39] the authors extended the reduced model in such a way that each fault is approximated by two distinct $(N-1)$-dimensional objects, one associated with each side of the fault. In the sequel we will refer to this type of approximation as a *double-layer reduced model* (DLRM) or (DL).

The main purpose of this article is to give a numerical discretization of the model proposed in [39] using the hybrid finite volume scheme [16, 15] modified to handle the fault flow. A comparison of the SLRM and the DLRM is given in the continuous as well as numerical context, showing their equivalence under suitable conditions. Moreover for both the reduced models, SLRM or DLRM, we prove an equivalence between their numerical approximation and what we call the "virtual fault cell" approach, avoiding the construction of the tangential operators. Several numerical examples are presented to show the robustness of the proposed method for both academic and realistic problems.

The paper is organized as follows: in Section 2 the notation and the governing equations of the physical problem are presented. In Section 3 the double-layer reduced model and the single-layer reduced model are derived and compared. Section 4 is devoted to the discretization of the proposed schemes, and some theoretical results, which may facilitate the implementation, are presented. In Section 5 a collection of examples highlights the possibilities of the proposed methods. Section 6 contains the conclusions. An appendix A, in which we briefly recall the derivation of the hybrid finite volume scheme for a standard diffusion problem, is included.

## 2 Flow in a domain with a fault

Throughout the rest of this article, unless otherwise specified, $i$, respectively $j$, will denote an index with values $i \in \{1, 2, f\}$, respectively $j \in \{1, 2\}$.

We consider as a computational domain a bounded, connected, open set $\Omega \subset \mathbb{R}^N$, $N = 2$ or 3, representing a porous medium.

We assume that $\Omega$ contains a fault $\Omega_f$, a connected, open subset of $\Omega$, and that $\Omega \setminus \overline{\Omega_f}$ is divided into two disjoint, connected, open subsets $\Omega_j$ as is shown in Figure 2. We denote by $\Gamma$ the boundary of $\Omega$, *i.e.* $\Gamma := \overline{\Omega} \setminus \Omega$, and by $\Gamma_i$ the external boundary of $\Omega_i$, *i.e.* $\Gamma_i := \partial\Omega_i \cap \Gamma$. The interface between the domain $\Omega_j$ and $\Omega_f$ is denoted by $\gamma_j$ and the unit normal vector field on $\gamma_j$ pointing outward from $\Omega_j$ is denoted by $\boldsymbol{n}_j$ . We suppose that the fault has a central axis $\hat{\gamma}$, a non self-intersecting $(N-1)$-dimensional surface, such that

$$\Omega_f = \left\{ \boldsymbol{x} \in \mathbb{R}^N : \boldsymbol{x} = \boldsymbol{s} + r\boldsymbol{n},\ \boldsymbol{s} \in \hat{\gamma},\ |r| < \frac{d}{2} \right\},$$

where $d$ is the thickness of $\Omega_f$ and $\boldsymbol{n}$ is the continuous unit normal vector field on $\hat{\gamma}$, pointing outward from $\Omega_1$ toward $\Omega_2$. We assume that the thickness $d$ of $\Omega_f$ is small compared to its other dimensions.

Throughout the following, we indicate with a subscript $i$, or $j$ as appropriate, the restriction of data and unknown functions (scalar or vector) to the corresponding subdomain of $\Omega$.

Our purpose is to compute the steady pressure field $p$ and the velocity field, or Darcy velocity, $\boldsymbol{u}$ in the entire domain $\Omega$. We suppose that flow is governed by the law of mass conservation together with Darcy's law, and for simplicity we assume that the only boundary condition on $\Gamma$ is a homogeneous condition for the pressure:

$$\begin{aligned} &\nabla \cdot \boldsymbol{u} = q && \\ &\boldsymbol{u} + \Lambda \nabla p = \boldsymbol{0} && \text{in } \Omega \\ &p = 0 && \text{on } \Gamma. \end{aligned} \tag{1}$$

Here $\Lambda$ denotes the symmetric and positive definite permeability tensor in $\Omega$, and the scalar source term $q$ represents a possible volume source or sink. We write problem (1) as an equivalent transmission problem:

$$\begin{aligned} &\nabla \cdot \boldsymbol{u}_i = q_i && \\ &\boldsymbol{u}_i + \Lambda_i \nabla p_i = \boldsymbol{0} && \text{in } \Omega_i \\ &p_i = 0 && \text{on } \Gamma_i, \end{aligned} \tag{2a}$$

coupled with interface conditions:

$$\begin{aligned} &p_j = p_f && \\ &\boldsymbol{u}_j \cdot \boldsymbol{n}_j = \boldsymbol{u}_f \cdot \boldsymbol{n}_j && \text{on } \gamma_j. \end{aligned} \tag{2b}$$

We have supposed, following [32], that the permeability tensor in $\Omega_f$ can be written as $\Lambda_f = \lambda_{f,\boldsymbol{n}} \boldsymbol{N} + \lambda_{f,\boldsymbol{\tau}} \boldsymbol{T}$, where the projection matrix $\boldsymbol{N}$ in the direction normal to $\hat{\gamma}$ and the projection matrix $\boldsymbol{T}$ in the direction tangential to $\hat{\gamma}$ are defined as follows:

$$\boldsymbol{N} := \boldsymbol{n} \otimes \boldsymbol{n} \quad \text{and} \quad \boldsymbol{T} := \boldsymbol{I} - \boldsymbol{N}.$$

The demonstration of the well posedness of problem (1) in its mixed weak form can be found in any number of texts; see [11, 36, 14, 38].

## 3 A double-layer reduced model

We are interested in a reduced model in which the fault $\Omega_f$ is represented by an interface which is identified with its central axis $\hat{\gamma}$. However, since $\Omega_1$ can slip along the fault with respect to $\Omega_2$, or vice versa, following [39], we subdivide $\Omega_f$ into two disjoint layers $\Omega_{f_j}$, such that $\overline{\Omega_f} = \cup_j \overline{\Omega_{f_j}}$:

$$\Omega_{f_j} = \left\{ \boldsymbol{x} \in \mathbb{R}^N : \boldsymbol{x} = \boldsymbol{s} + r\boldsymbol{n},\ \boldsymbol{s} \in \hat{\gamma},\ r \in T_j \right\},$$

where $T_1 = (-d/2, 0)$ and $T_2 = (0, d/2)$ . Each layer $\Omega_{f_j}$, in turn has a central axis, a translation of $\hat{\gamma}$, which we denote by $\hat{\gamma}_j$. For a double-layer reduced model, a DLRM, each layer $\Omega_{f_j}$ is approximated by its central axis $\hat{\gamma}_j$. We first derive equations governing flow in $\hat{\gamma}_j$ and an equation coupling flow in $\hat{\gamma}_j$ with flow in $\Omega_j$. These equations are derived similarly to the corresponding equations in the single-layer reduced model, the SLRM. Then to complete the

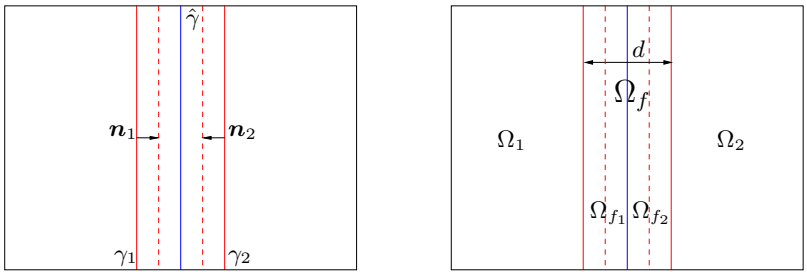



Figure 2: Representation of each sub-domain.

model we derive an equation coupling flow in $\hat{\gamma}_1$ with flow in $\hat{\gamma}_2$, as in the final model $\hat{\gamma}, \hat{\gamma}_1$ and $\hat{\gamma}_2$ are all identified with each other. To obtain the equations describing flow on $\hat{\gamma}_j$ we integrate the equations for flow in $\Omega_f$, (2a), across normal cross sections of $\Omega_{f_j}$. However, we first split the vector terms into their normal and tangential parts. To do this we will make use of the normal and tangential divergence and gradient operators:

$$\nabla_{\boldsymbol{n}} \cdot := \boldsymbol{N} : \nabla \quad \text{and} \quad \nabla_{\boldsymbol{\tau}} \cdot := \boldsymbol{T} : \nabla,$$
$$\nabla_{\boldsymbol{n}} := \boldsymbol{N}\nabla \quad \text{and} \quad \nabla_{\boldsymbol{\tau}} := \boldsymbol{T}\nabla,$$

and we will write the Darcy velocity in $\Omega_f$ as a sum of its normal and tangential components:

$$\boldsymbol{u}_f = \boldsymbol{N}\boldsymbol{u}_f + \boldsymbol{T}\boldsymbol{u}_f = \boldsymbol{u}_{f,\boldsymbol{n}} + \boldsymbol{u}_{f,\boldsymbol{\tau}}$$

with $\boldsymbol{u}_{f,\boldsymbol{n}} := \boldsymbol{N}\boldsymbol{u}_f$ and $\boldsymbol{u}_{f,\boldsymbol{\tau}} := \boldsymbol{T}\boldsymbol{u}_f$. We will use the hat notation $\hat{\cdot}$ to denote reduced functions, *i.e.* functions defined on $\hat{\gamma}_1$ or $\hat{\gamma}_2$ in the reduced model. The reduced source term on $\hat{\gamma}_j$ is defined to be $\hat{q}_j := \int_{T_j} q_f$, while the reduced (tangential) Darcy velocity along $\hat{\gamma}_j$ is $\hat{\boldsymbol{u}}_j := \int_{T_j} \boldsymbol{u}_{f,\boldsymbol{\tau}}$. Then integrating the conservation equation, the second equation of (2a), across normal cross sections of $\Omega_{f_j}$ we obtain

$$\int_{T_j} \nabla \cdot \boldsymbol{u}_f = \boldsymbol{u}_f \cdot \boldsymbol{n}|_{\hat{\gamma}} - \boldsymbol{u}_f \cdot \boldsymbol{n}|_{\gamma_j} + \nabla_{\boldsymbol{\tau}} \cdot \hat{\boldsymbol{u}}_j = \hat{q}_j$$

which we may now write as

$$\nabla_{\boldsymbol{\tau}} \cdot \hat{\boldsymbol{u}}_j = \hat{q}_j + [\![\boldsymbol{u} \cdot \boldsymbol{n}]\!]_{\gamma_j} \quad \text{in } \hat{\gamma}_j, \tag{3}$$

where we have introduced the flux jump $[\![\boldsymbol{u} \cdot \boldsymbol{n}]\!]_{\gamma_j}$ across $\hat{\gamma}_j$ defined by

$$\begin{aligned}[\![\boldsymbol{u} \cdot \boldsymbol{n}]\!]_{\gamma_j} :=& (-1)^j (\boldsymbol{u}_f \cdot \boldsymbol{n}|_{\hat{\gamma}} - \boldsymbol{u}_f \cdot \boldsymbol{n}|_{\gamma_j}) \\ =& (-1)^j \left( \hat{u}_{\boldsymbol{n}} - \boldsymbol{u}_j \cdot \boldsymbol{n}|_{\gamma_j} \right).\end{aligned}$$

For the second equality we have used the continuity of the flux at $\gamma_j$, the second equation of (2b), and have introduced the notation $\hat{u}_{\boldsymbol{n}}$ for $\boldsymbol{u}_f \cdot \boldsymbol{n}|_{\hat{\gamma}}$.

We consider now Darcy's law in the fault $\Omega_f$ and split it into its normal and tangential components:

$$\boldsymbol{u}_{f,\boldsymbol{n}} = -\lambda_{f,\boldsymbol{n}} \nabla_{\boldsymbol{n}} p_f$$
$$\boldsymbol{u}_{f,\boldsymbol{\tau}} = -\lambda_{f,\boldsymbol{\tau}} \nabla_{\boldsymbol{\tau}} p_f.$$

To derive a reduced form of Darcy's law on $\hat{\gamma}_j$ we will need the reduced pressure $\hat{p}_j$ and the reduced permeability $\hat{\lambda}$ defined by

$$\hat{p}_j := \frac{2}{d} \int_{T_j} p_f \quad \text{and} \quad \hat{\lambda} := d \frac{\lambda_{f,\boldsymbol{\tau}}}{2}.$$

Considering the tangential part of Darcy's law and integrating it across normal cross sections of each layer of the fault we obtain

$$\hat{\boldsymbol{u}}_j = -\hat{\lambda} \nabla_{\boldsymbol{\tau}} \hat{p}_j, \quad \text{in } \hat{\gamma}_j. \tag{4}$$

The normal part of Darcy's law can now be used to derive a condition coupling flow in $\hat{\gamma}_j$ with flow in $\Omega_j$. We integrate over the normal cross sections of the outer half of the layer $\Omega_{f_j}$ and use the first equation of (2b), the continuity condition for the pressure at the interface $\gamma_j$, to obtain

$$\int_a^b \boldsymbol{u}_{f,\boldsymbol{n}} \cdot \boldsymbol{n} = (-1)^j \lambda_{f,\boldsymbol{n}} (\hat{p}_j - p_j),$$

where $a$ and $b$ are respectively $-\frac{d}{2}$ and $-\frac{d}{4}$ if $j=1$ and $\frac{d}{4}$ and $\frac{d}{2}$ if $j=2$. Approximating the integral in the preceding equation as follows:

$$\int_a^b \boldsymbol{u}_{f,\boldsymbol{n}} \cdot \boldsymbol{n} \approx \frac{d}{4}\, \boldsymbol{u}_{f,\boldsymbol{n}} \cdot \boldsymbol{n}|_{\gamma_j},$$

and using the continuity condition for the normal component of the velocity, the second equation of (2b), we obtain the coupling condition

$$\boldsymbol{u}_j \cdot \boldsymbol{n} = (-1)^j 2\hat{\lambda}_{\boldsymbol{n}} \left(\hat{p}_j - p_j\right), \quad \text{on } \hat{\gamma}_j, \tag{5}$$

where $\hat{\lambda}_{\boldsymbol{n}} := \dfrac{2}{d}\lambda_{f,\boldsymbol{n}}$.

Now even though $\hat{\gamma}_j$ and $\hat{\gamma}$ are, in the DLRM, in fact the same interface, they are thought of as being different sides of the interface, and two distinct flows (Darcy velocities and pressures) $(\hat{\boldsymbol{u}}_j, \hat{p}_j)$ are calculated, so an additional equation is now needed to express the coupling between the two sides of the fault. To obtain this we consider again the normal component of the Darcy equation in $\Omega_f$ and this time integrate across the normal cross sections of the inner halves of the two layers $\Omega_{f_1}$ and $\Omega_{f_2}$:

$$\int_{-\frac{d}{4}}^{\frac{d}{4}} \boldsymbol{u}_{f,\boldsymbol{n}} \cdot \boldsymbol{n} = -\lambda_{f,\boldsymbol{n}} \left(\hat{p}_2 - \hat{p}_1\right).$$

Then using a mid-point rule to approximate the integral of $\boldsymbol{u}_{f,\boldsymbol{n}} \cdot \boldsymbol{n}$,

$$\int_{-\frac{d}{4}}^{\frac{d}{4}} \boldsymbol{u}_{f,\boldsymbol{n}} \cdot \boldsymbol{n} \approx \frac{d}{2}\, \boldsymbol{u}_f \cdot \boldsymbol{n}|_{\hat{\gamma}} = \frac{d}{2}\hat{u}_{\boldsymbol{n}},$$

we obtain the condition

$$\hat{u}_{\boldsymbol{n}} = \hat{\lambda}_{\boldsymbol{n}} \left[\!\left[\hat{p}\right]\!\right]_{\hat{\gamma}}, \tag{6}$$

where $\left[\!\left[\hat{p}\right]\!\right]_{\hat{\gamma}} := \hat{p}_1 - \hat{p}_2$.

Collecting the equations (2a) for flow in $\Omega_j$, (3) and (4) for flow in the reduced fault layers $\hat{\gamma}_j$, and the coupling conditions (5) and (6) we obtain the double-layer reduced model: for the porous medium domains $\Omega_j$

$$\begin{aligned} &\nabla \cdot \boldsymbol{u}_j = q_j && \\ &\boldsymbol{u}_j = -\Lambda_j \nabla p_j && \text{in } \Omega_j \\ &p_j = 0 && \text{on } \Gamma_j \end{aligned}, \tag{7a}$$

for the two reduced layers of the fault

$$\begin{aligned} &\nabla_{\boldsymbol{\tau}} \cdot \hat{\boldsymbol{u}}_j = \hat{q}_j + \left[\!\left[\boldsymbol{u} \cdot \boldsymbol{n}\right]\!\right]_{\gamma_j} && \\ &\hat{\boldsymbol{u}}_j = -\hat{\lambda} \nabla_{\boldsymbol{\tau}} \hat{p}_j && \text{in } \hat{\gamma}_j \\ &\hat{p}_j = 0 && \text{on } \partial\hat{\gamma}_j \end{aligned}, \tag{7b}$$

with the coupling conditions

$$\begin{aligned} \boldsymbol{u}_1 \cdot \boldsymbol{n} &= 2\hat{\lambda}_{\boldsymbol{n}} \left(p_1 - \hat{p}_1\right) && \text{on } \hat{\gamma}_1 \\ \boldsymbol{u}_2 \cdot \boldsymbol{n} &= 2\hat{\lambda}_{\boldsymbol{n}} \left(\hat{p}_2 - p_2\right) && \text{on } \hat{\gamma}_2 \\ \hat{u}_{\boldsymbol{n}} &= \hat{\lambda}_{\boldsymbol{n}} \left[\!\left[\hat{p}\right]\!\right]_{\hat{\gamma}} && \text{on } \hat{\gamma}. \end{aligned} \tag{7c}$$

As mentioned earlier, while constructing the DLRM we have distinguished 3 different interfaces, $\hat{\gamma}_1, \hat{\gamma}$, and $\hat{\gamma}_2$, which are all in fact in the final model associated with the same interface-domain. An alternative form of (7c) can thus be obtained by considering the three equations to be equations on the same interface $\hat{\gamma}$ and adding and subtracting the first two equations to obtain an equivalent version of the coupling conditions on $\hat{\gamma}$:

$$\begin{aligned} \left\{\!\!\left\{\boldsymbol{u} \cdot \boldsymbol{n}\right\}\!\!\right\}_{\hat{\gamma}} &= \hat{\lambda}_{\boldsymbol{n}} \left(\left[\!\left[p\right]\!\right]_{\hat{\gamma}} - \left[\!\left[\hat{p}\right]\!\right]_{\hat{\gamma}}\right) \\ \left[\!\left[\boldsymbol{u} \cdot \boldsymbol{n}\right]\!\right]_{\hat{\gamma}} &= 4\hat{\lambda}_{\boldsymbol{n}} \left(\left\{\!\!\left\{p\right\}\!\!\right\}_{\hat{\gamma}} - \left\{\!\!\left\{\hat{p}\right\}\!\!\right\}_{\hat{\gamma}}\right) \\ \hat{u}_{\boldsymbol{n}} &= \hat{\lambda}_{\boldsymbol{n}} \left[\!\left[\hat{p}\right]\!\right]_{\hat{\gamma}}. \end{aligned} \tag{7c-bis}$$

Here the mean operators are defined by

$$\left\{\!\!\left\{\boldsymbol{u} \cdot \boldsymbol{n}\right\}\!\!\right\}_{\hat{\gamma}} := \frac{1}{2}\left(\boldsymbol{u}_1 \cdot \boldsymbol{n}|_{\hat{\gamma}} + \boldsymbol{u}_2 \cdot \boldsymbol{n}|_{\hat{\gamma}}\right)$$
$$\left\{\!\!\left\{p\right\}\!\!\right\}_{\hat{\gamma}} := \frac{1}{2}\left(p_1|_{\hat{\gamma}} + p_2|_{\hat{\gamma}}\right)$$

and the jump operators by

$$\left[\!\left[\boldsymbol{u} \cdot \boldsymbol{n}\right]\!\right]_{\hat{\gamma}} := \boldsymbol{u}_1 \cdot \boldsymbol{n}|_{\hat{\gamma}} - \boldsymbol{u}_2 \cdot \boldsymbol{n}|_{\hat{\gamma}}$$
$$\left[\!\left[p\right]\!\right]_{\hat{\gamma}} := p_1|_{\hat{\gamma}} - p_2|_{\hat{\gamma}}.$$

We remark that one can consider different values of $\hat{\lambda}$ and $\hat{\lambda}_{\boldsymbol{n}}$ for each layer but, for simplicity of exposition, we have not done this here. However, in Section 5.3 we give an example with different values of $\hat{\lambda}$ for each layer of the fault.

The numerical discretization that we will use for the approximation of (7) is based on a weak formulation which we now define. Let

$\mathcal{V} := \prod_{j=1}^{2} \mathcal{V}_j$, where $\mathcal{V}_j := H^1_\Gamma(\Omega_j)$ is the space of those functions in $H^1(\Omega_j)$ having a vanishing trace on $\partial\Omega_j \cap \Gamma$ and $\hat{\mathcal{V}} := \prod_{j=1}^{2} \hat{\mathcal{V}}_j$, where $\hat{\mathcal{V}}_j = H^1_\Gamma(\hat{\gamma})$ is the space of functions in $H^1(\hat{\gamma})$ having a vanishing trace on $\partial\hat{\gamma} \cap \Gamma$. We then define the bilinear forms $a_\Omega$ and $a_{\hat{\gamma}}$ on $\mathcal{V} \times \mathcal{V}$ and $\hat{\mathcal{V}} \times \hat{\mathcal{V}}$, respectively by

$$a_\Omega(p, v) := \sum_{j=1,2} (\Lambda_j \nabla p_j, \nabla v_j)_{\Omega_j}, \tag{8}$$

and

$$a_{\hat{\gamma}}(\hat{p}, \hat{v}) := \sum_{j=1,2} \left(\hat{\lambda} \nabla_{\boldsymbol{\tau}} \hat{p}_j, \nabla_{\boldsymbol{\tau}} \hat{v}_j\right)_{\hat{\gamma}_j}, \tag{9}$$

and the global diffusion bilinear form $a$ is defined on $(\mathcal{V} \times \hat{\mathcal{V}}) \times (\mathcal{V} \times \hat{\mathcal{V}})$ by

$$a\big((p, \hat{p}), (v, \hat{v})\big) := a_\Omega(p, v) + a_{\hat{\gamma}}(\hat{p}, \hat{v}).$$

To enforce the coupling conditions (7c) in the weak formulation we need another bilinear form. Let $cc$ denote the bilinear form defined on $(\mathcal{V} \times \hat{\mathcal{V}}) \times (\mathcal{V} \times \hat{\mathcal{V}})$ by

$$\begin{aligned} cc\big((p, \hat{p}), (v, \hat{v})\big) &:= \left(\hat{\lambda}_{\boldsymbol{n}} [\![\hat{p}]\!]_{\hat{\gamma}}, [\![\hat{v}]\!]_{\hat{\gamma}}\right)_{\hat{\gamma}} \\ &+ \sum_{j=1,2} 2\left(\hat{\lambda}_{\boldsymbol{n}} p_j - \hat{\lambda}_{\boldsymbol{n}} \hat{p}_j, v_j - \hat{v}_j\right)_{\hat{\gamma}_j}, \end{aligned} \tag{10}$$

which using (7c-bis) may alternatively be written as

$$\begin{aligned} cc\big((p, \hat{p}), (v, \hat{v})\big) &:= \left(\hat{\lambda}_{\boldsymbol{n}} [\![\hat{p}]\!]_{\hat{\gamma}}, [\![\hat{v}]\!]_{\hat{\gamma}}\right)_{\hat{\gamma}} \\ &+ 4\left(\hat{\lambda}_{\boldsymbol{n}} \{\!\{p\}\!\}_{\hat{\gamma}} - \hat{\lambda}_{\boldsymbol{n}} \{\!\{\hat{p}\}\!\}_{\hat{\gamma}}, \{\!\{v\}\!\}_{\hat{\gamma}} - \{\!\{\hat{v}\}\!\}_{\hat{\gamma}}\right)_{\hat{\gamma}} \\ &+ \left(\hat{\lambda}_{\boldsymbol{n}} [\![p]\!]_{\hat{\gamma}} - \hat{\lambda}_{\boldsymbol{n}} [\![\hat{p}]\!]_{\hat{\gamma}}, [\![v]\!]_{\hat{\gamma}} - [\![\hat{v}]\!]_{\hat{\gamma}}\right)_{\hat{\gamma}}. \end{aligned} \tag{10-bis}$$

The right-hand side functional $F$ is defined on $\mathcal{V} \times \hat{\mathcal{V}}$ by

$$F(v, \hat{v}) := \sum_{j=1,2} (q_j, v_j)_{\Omega_j} + \sum_{j=1,2} (\hat{q}_j, \hat{v}_j)_{\hat{\gamma}_j}.$$

The weak formulation of (7) may be written as follows:

$$\begin{aligned} &\text{find } (p, \hat{p}) \in \mathcal{V} \times \hat{\mathcal{V}} \text{ such that} \\ &a\big((p, \hat{p}), (v, \hat{v})\big) + cc\big((p, \hat{p}), (v, \hat{v})\big) = F(v, \hat{v}), \\ &\text{for all } (v, \hat{v}) \in \mathcal{V} \times \hat{\mathcal{V}}. \end{aligned} \tag{11}$$

We point out that the SLRM in [32, 12], with a suitable choice of the weighting parameter, can be recovered by requiring that $\hat{p}_1 = \hat{p}_2$, which implies that $\hat{\boldsymbol{u}}_1 = \hat{\boldsymbol{u}}_2$, and that $\hat{u}_{\boldsymbol{n}} = (\boldsymbol{u}_1 \cdot \boldsymbol{n} + \boldsymbol{u}_2 \cdot \boldsymbol{n})/2 + (\hat{q}_1 - \hat{q}_2)/2$. This however is equivalent to collapsing the interior half of the fault resulting in a fault of half the width. Thus to maintain the full width of the fault every occurrence of $d$ should be replaced by $2d$ or more to the point, every occurrence of $\hat{\lambda}$ by $2\hat{\lambda}$ and every occurrence of $\hat{\lambda}_{\boldsymbol{n}}$ by $\hat{\lambda}_{\boldsymbol{n}}/2$. Thus, now writing $\hat{p}$ for $\hat{p}_j$, $\hat{\boldsymbol{u}}$ for $\hat{\boldsymbol{u}}_1 + \hat{\boldsymbol{u}}_2$ and $\hat{q}$ for $\hat{q}_1 + \hat{q}_2$, the SLRM can be written as follows: for the porous medium domains $\Omega_j$

$$\begin{aligned} &\nabla \cdot \boldsymbol{u}_j = q_j && \\ &\boldsymbol{u}_j = -\Lambda_j \nabla p_j && \text{in } \Omega_j \\ &p = 0 && \text{on } \Gamma_j \end{aligned} \tag{12a}$$

for the the reduced fault $\hat{\gamma}$

$$\begin{aligned} &\nabla_{\boldsymbol{\tau}} \cdot \hat{\boldsymbol{u}} = \hat{q} + [\![\boldsymbol{u} \cdot \boldsymbol{n}]\!]_{\hat{\gamma}} && \\ &\hat{\boldsymbol{u}} = -2\hat{\lambda} \nabla_{\boldsymbol{\tau}} \hat{p} && \text{in } \hat{\gamma} \\ &\hat{p} = 0 && \text{on } \partial\hat{\gamma} \end{aligned} \tag{12b}$$

with the coupling conditions

$$\begin{aligned} &\{\!\{\boldsymbol{u} \cdot \boldsymbol{n}\}\!\}_{\hat{\gamma}} = \frac{\hat{\lambda}_{\boldsymbol{n}}}{2} [\![p]\!]_{\hat{\gamma}} \\ &[\![\boldsymbol{u} \cdot \boldsymbol{n}]\!]_{\hat{\gamma}} = 2\hat{\lambda}_{\boldsymbol{n}} \left(\{\!\{p\}\!\}_{\hat{\gamma}} - \hat{p}\right) \end{aligned} \quad \text{on } \hat{\gamma}. \tag{12c}$$

Note that in the case of the SLRM the weak formulation of (7) is modified as follows: the space $\mathcal{V}$ is unchanged, the space $\hat{\mathcal{V}}$ is replaced by a single copy (instead of two) of $H^1_\Gamma(\hat{\gamma})$, in the two bilinear forms making up $a((\cdot,\cdot),(\cdot,\cdot))$ the bilinear form $a_\Omega(\cdot,\cdot)$ is unchanged, and the bilinear form $a_{\hat{\gamma}}(\cdot,\cdot)$ is modified by removing the sum over $j$ and dropping the index $j$, and multiplying by 2:

$$a_{\hat{\gamma}}(\hat{p}, \hat{v}) := 2\left(\hat{\lambda} \nabla_{\boldsymbol{\tau}} \hat{p}, \nabla_{\boldsymbol{\tau}} \hat{v}\right)_{\hat{\gamma}}. \tag{13}$$

For the SLRM the bilinear form for the coupling simplifies to

$$\begin{aligned} cc\big((p, \hat{p}), (v, \hat{v})\big) &:= \frac{1}{2}\left(\hat{\lambda}_{\boldsymbol{n}} [\![p]\!]_{\hat{\gamma}}, [\![v]\!]_{\hat{\gamma}}\right)_{\hat{\gamma}} \\ &+ 2\left(\hat{\lambda}_{\boldsymbol{n}} (\{\!\{p\}\!\}_{\hat{\gamma}} - \hat{p}), (\{\!\{v\}\!\}_{\hat{\gamma}} - \hat{v})\right)_{\hat{\gamma}}. \end{aligned} \tag{14}$$

# 4 Numerical approximation

The numerical approximation of the proposed models is the main part of this work. For the derivation of the approximation, we will consider only planar faults and faces although some numerical results with non-planar faults are shown in Section 5. In the first subsection we briefly recall the hybrid finite volume (HFV) scheme which is the basis for the numerical scheme we use, (a more thorough description is given in Appendix A.2) and show how this scheme can be extended to approximate a reduced fault model. Then follows an exposition of approximation using the *virtual fault cells* approach. The final subsection is devoted to a comparison of the two discretization techniques.

## 4.1 Discretization with the HFV scheme

To solve numerically (7) and (12) we use the hybrid finite volume (HFV) scheme, introduced in [16, 13]. First we recall what is meant by a HFV discretization of an open set $\mathcal{O} \subset \mathbb{R}^N$ for $N = 1, 2, 3$.

**Definition 1** (Discretization of $\mathcal{O}$)**.** *For $\mathcal{O}$ an open set in $\mathbb{R}^N$, a discretization of $\mathcal{O}$, denoted by $\mathcal{D}$ is defined to be a triple $\mathcal{D} := (\mathcal{M}, \mathcal{E}, \mathcal{P})$ where*

1. *$\mathcal{M}$ is a set of cells or control volumes; i.e. a set of disjoint, non-empty, open, polyhedra if $N = 3$, polygons if $N = 2$, or line segments if $N = 1$, lying in $\mathcal{O}$ such that*

$$\overline{\mathcal{O}} = \bigcup_{K \in \mathcal{M}} \overline{K}. \tag{15}$$

   *For $K$ a cell, let $|K| > 0$ denote the measure of $K$.*

2. *$\mathcal{E}$ is the set of the $(N-1)$-dimensional faces of the cells in $\mathcal{M}$. The set $\mathcal{E}$ is divided into the set of external faces $\mathcal{E}_{\text{ext}} = \{\sigma \in \mathcal{E} : E \subset \partial\mathcal{O}\}$, and the set of internal faces $\mathcal{E}_{\text{int}} = \{\sigma \in \mathcal{E} : E \subset \mathcal{O}\}$. We have $\mathcal{E} = \mathcal{E}_{\text{int}} \cup \mathcal{E}_{\text{ext}}$. For $\sigma \in \mathcal{E}$, $|\sigma| > 0$ will denote the measure of $\sigma$. We assume $|\sigma| = 1$ if $N = 1$. For each cell $K \in \mathcal{M}$, we denote by $\mathcal{E}_K \subset \mathcal{E}$ the set of all $(N-1)$-dimensional faces of $K$ and for each face $\sigma \in \mathcal{E}$ we denote by $\mathcal{M}_\sigma := \{K \in \mathcal{M} : \sigma \in \mathcal{E}_K\}$ the set of all cells in $\mathcal{M}$ having $\sigma$ as a face;*

3. *$\mathcal{P}$ is the set of points, defined by $\mathcal{P} := \{\boldsymbol{x}_K : K \in \mathcal{M}\} \cup \{\boldsymbol{x}_\sigma : \sigma \in \mathcal{E}\}$, where $\boldsymbol{x}_K$ is the barycentre of the cell $K \in \mathcal{M}$ and $\boldsymbol{x}_\sigma$ is the barycentre of the face $\sigma \in \mathcal{E}$;*

4. *for each cell $K \in \mathcal{M}$ and face $\sigma \in \mathcal{E}_K$, we indicate by $\boldsymbol{n}_{K,\sigma}$ the unit vector normal to $\sigma$ pointing outward from $K$;*

5. *for each cell $K \in \mathcal{M}$ and face $\sigma \in \mathcal{E}_K$ we denote by $D_{K,\sigma} \subset K$ the cone with vertex $\boldsymbol{x}_K$ and base $\sigma$ and by $d_{K,\sigma} \in \mathbb{R}^+$ the orthogonal distance between $\boldsymbol{x}_K$ and $\sigma$.*

To obtain a HFV discretization of a domain with a fault we extend this definition to the case of an open set $\Omega \subset \mathbb{R}^N$, for $N = 2, 3$, which is divided into the subdomains $\Omega_1$ and $\Omega_2$ by an interface (planar if $N = 3$, linear if $N = 2$) fault $\hat{\gamma}$.

**Definition 2** (Discretization of $(\Omega, \hat{\gamma})$)**.** *For a domain $\Omega \subset \mathbb{R}^N$ divided into the subdomains $\Omega_1$ and $\Omega_2$ by an interface fault $\hat{\gamma}$, we construct a discretization $(\mathcal{D}, \hat{\mathcal{D}})$ from discretizations $\mathcal{D}_j = (\mathcal{M}_j, \mathcal{E}_j, \mathcal{P}_j)$ of $\Omega_j$ and from, in the case of the SLRM, a discretization $\hat{\mathcal{D}} = (\hat{\mathcal{M}}, \hat{\mathcal{E}}, \hat{\mathcal{P}})$ of $\hat{\gamma}$ or in the case of the DLRM, discretizations $\hat{\mathcal{D}}_j = (\hat{\mathcal{M}}_j, \hat{\mathcal{E}}_j, \hat{\mathcal{P}}_j)$ of $\hat{\gamma}_j$, where $\hat{\gamma}_j$ is the part of the boundary of $\Omega_j$ lying on the fault $\hat{\gamma}$. Then $\mathcal{D}$ is defined to be*

$$\begin{aligned}
&\mathcal{D} = (\mathcal{M}, \mathcal{E}, \mathcal{P}) \text{ where} \\
&\mathcal{M} = \mathcal{M}_1 \cup \mathcal{M}_2,\ \mathcal{E} = \mathcal{E}_1 \cup \mathcal{E}_2,\ \mathcal{P} = \mathcal{P}_1 \cup \mathcal{P}_2,
\end{aligned}$$

*and $\hat{\mathcal{D}}$ is defined by*

$$\begin{aligned}
&\text{in the case of the SLRM} \\
&\hat{\mathcal{D}} = (\hat{\mathcal{M}}, \hat{\mathcal{E}}, \hat{\mathcal{P}}) \text{ as given} \\
&\text{or in the case of the DLRM} \\
&\hat{\mathcal{D}} = (\hat{\mathcal{M}}, \hat{\mathcal{E}}, \hat{\mathcal{P}}) \text{ where} \\
&\hat{\mathcal{M}} = \hat{\mathcal{M}}_1 \cup \hat{\mathcal{M}}_2,\ \hat{\mathcal{E}} = \hat{\mathcal{E}}_1 \cup \hat{\mathcal{E}}_2,\ \hat{\mathcal{P}} = \hat{\mathcal{P}}_1 \cup \hat{\mathcal{P}}_2,
\end{aligned}$$

*Denote by $\mathcal{E}_{j,\text{int}}$, the set of internal faces of $\mathcal{E}_j$, and divide the external faces of $\mathcal{E}_j$ into $\mathcal{E}_{j,\Gamma}$, the set of faces lying on the boundary $\Gamma$ of $\Omega$, and $\mathcal{E}_{j,\hat{\gamma}}$, the set of those lying on the fault $\hat{\gamma}$.*

*For the SLRM, if $\hat{K} \in \hat{\mathcal{M}}$, a face in $\mathcal{E}_{j,\hat{\gamma}}$ coinciding with $\hat{K}$ will be denoted $\sigma_{\hat{K},j}$ while for the DLRM if $\hat{K}_j \in \hat{\mathcal{M}}_j$, a face in $\mathcal{E}_{j,\hat{\gamma}}$ coinciding with $\hat{K}_j$ will be denoted $\sigma_{\hat{K}_j}$.*

*For the SLRM we will say that the discretization $(\mathcal{D}, \hat{\mathcal{D}})$ is conforming if the set of control volumes $\hat{\mathcal{M}}$ is identical to both the set of faces $\mathcal{E}_{1,\hat{\gamma}}$ and the set of faces $\mathcal{E}_{2,\hat{\gamma}}$; i.e. the discretizations $\mathcal{D}_1$ and $\mathcal{D}_2$ match up along $\hat{\gamma}$, and the discretization on $\hat{\gamma}$ is inherited from each of the discretizations $\mathcal{D}_1$ and $\mathcal{D}_2$. In the case of the DLRM, the discretization $(\mathcal{D}, \hat{\mathcal{D}})$ is said to be conforming if the set of cells in $\hat{\mathcal{M}}_j$ is identical with the set of faces $\mathcal{E}_{j,\hat{\gamma}}$. However, the two discretizations $\hat{\mathcal{D}}_j$ (when viewed as discretizations on $\hat{\gamma}_j$) are not required to be identical.*

See Figure 3 for an example of meshes. For a discretization $(\mathcal{D}, \hat{\mathcal{D}})$, the pressure in the matrix is approximated by a scalar value $p_K$ in each cell $K \in \mathcal{M}$ and by a scalar value $p_\sigma$ for each face $\sigma \in \mathcal{E}$. Similarly, the pressure in the fault is approximated by a scalar value $\hat{p}_{\hat{K}}$ in each cell $\hat{K} \in \hat{\mathcal{M}}$ and by a scalar value $\hat{p}_{\hat{\sigma}}$ on each face $\hat{\sigma} \in \hat{\mathcal{E}}$. So the discrete solution which we will denote $(p, \hat{p})$, with apologies for the abuse of notation, associated with $(\mathcal{D}, \hat{\mathcal{D}})$ is of the form

$$p = ((p_K)_{K\in\mathcal{M}}, (p_\sigma)_{\sigma\in\mathcal{E}})$$
$$\hat{p} = \left((\hat{p}_{\hat{K}})_{\hat{K}\in\hat{\mathcal{M}}}, (\hat{p}_{\hat{\sigma}})_{\hat{\sigma}\in\hat{\mathcal{E}}}\right)$$

with $p_K, p_\sigma, \hat{p}_{\hat{K}}$, and $\hat{p}_{\hat{\sigma}}$ representing an approximation of the average value of $p$ in $K, \sigma, \hat{K}$ and $\hat{\sigma}$, respectively. Thus for the SLRM with a conforming discretization $(\mathcal{D}, \hat{\mathcal{D}})$, a cell $\hat{K} \in \hat{\mathcal{M}}$ is also both a face $\sigma_1 \in \mathcal{E}_{1,\hat{\gamma}}$ and a face $\sigma_2 \in \mathcal{E}_{2,\hat{\gamma}}$ and will thus be associated with three values $\hat{p}_{\hat{K}}, p_{\sigma_1}$ and $p_{\sigma_2}$. Similarly for the DLRM with a conforming discretization $(\mathcal{D}, \hat{\mathcal{D}})$, if a cell in $\hat{\mathcal{M}}_1$ is also a cell in $\hat{\mathcal{M}}_2$ it will be associated with four values; cf. Figure 4.

The discrete problem for the HFV scheme is based on the variational form of the continuous problem (11) and requires the definition of a discrete gradient. Once the discrete gradient

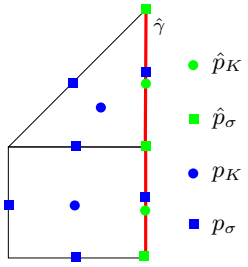



Figure 4: Example of a mesh for $(\Omega, \hat{\gamma})$ with a representation of the *d.o.f.*'s. In the case of the DLRM the *d.o.f.*'s in the fault are doubled.

$\nabla_{\mathcal{D}}$ is defined the bilinear form (8) is approximated by replacing the gradient with the discrete gradient in its definition. To define the discrete gradient operator we begin by defining for each $K \in \mathcal{M}$ a cell gradient:

$$\nabla_K p := \frac{1}{|K|} \sum_{\sigma\in\mathcal{E}_K} |\sigma| (p_\sigma - p_K) \boldsymbol{n}_{K,\sigma}$$

and for each face $\sigma \in \mathcal{E}_K$ a stabilization term for the cone $D_{K,\sigma}$ with vertex $\boldsymbol{x}_K$ and base $\sigma$ ($D_{K,\sigma} \subset K$):

$$R_{K,\sigma}p := \frac{\beta}{d_{K,\sigma}} \left[p_\sigma - p_K - \nabla_K p \cdot (\boldsymbol{x}_\sigma - \boldsymbol{x}_K)\right],$$

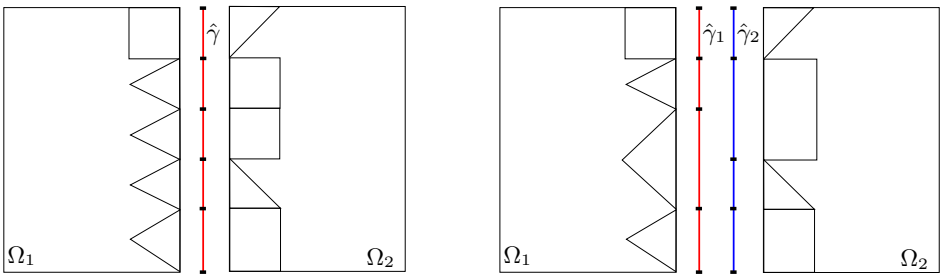
where $\beta = \sqrt{\alpha N}$, and $\alpha \in \mathbb{R}^+$ is a stabilization parameter which can vary from cell to cell. Then the discrete gradient for the matrix domain is defined by

$$\nabla_{\mathcal{D}} p|_{D_{K,\sigma}} := \nabla_K p + R_{K,\sigma}p \, \boldsymbol{n}_{K,\sigma}.$$

The discrete gradient $\nabla_{\mathcal{D}} p$ is thus piecewise constant, constant on each cone $D_{K,\sigma}$, $K \in \mathcal{M}, \sigma \in \mathcal{E}_{K,\sigma}$. See Appendix A.2 for more details.

For implementation in the SLRM or DLRM we also need a discrete (tangential) gradient in the fault which is defined similarly. Once the discrete tangential gradient $\hat{\nabla}_{\mathcal{D}}$ is defined the bilinear form (9) is approximated by replacing the tangential gradient with the discrete tangential gradient in its definition. For each $\hat{K} \in \hat{\mathcal{M}}$, the (fault) cell gradient is defined by

$$\hat{\nabla}_{\hat{K}} \hat{p} := \frac{1}{|\hat{K}|} \sum_{\hat{\sigma}\in\hat{\mathcal{E}}_{\hat{K}}} |\hat{\sigma}| \left(\hat{p}_{\hat{\sigma}} - \hat{p}_{\hat{K}}\right) \hat{\boldsymbol{n}}_{\hat{K},\hat{\sigma}}, \quad (16)$$




(a) SLRM (b) DLRM

Figure 3: Example of cells adjacent to the fault for the SLRM and DLRM. These represent conforming meshes in the sense that the fault mesh is inherited from the domain mesh.

and for each $\hat{\sigma} \in \hat{\mathcal{E}}_{\hat{K}}$ the stabilization term $R_{\hat{K},\hat{\sigma}}$ is defined on the cone $D_{\hat{K},\hat{\sigma}}$ by

$$R_{\hat{K},\hat{\sigma}}\hat{p} := \frac{\hat{\beta}}{d_{\hat{K},\hat{\sigma}}}\left[\hat{p}_{\hat{\sigma}} - \hat{p}_{\hat{K}} - \hat{\nabla}_{\hat{K}}\hat{p}\cdot\left(\boldsymbol{x}_{\hat{\sigma}} - \boldsymbol{x}_{\hat{K}}\right)\right], \tag{17}$$

where $\hat{\beta} = \sqrt{\hat{\alpha}(N-1)}$ and $\hat{\alpha} \in \mathbb{R}^+$ is a stabilization parameter for the fault cell $\hat{K}$. Then, as in the matrix, the discrete (tangential) gradient for the fault domain $\hat{\gamma}$ is defined cone by cone:

$$\hat{\nabla}_{\mathcal{D}}\,\hat{p}\Big|_{D_{\hat{K},\hat{\sigma}}} := \hat{\nabla}_{\hat{K}}\,\hat{p} + R_{\hat{K},\hat{\sigma}}\hat{p}\,\hat{\boldsymbol{n}}_{\hat{K},\hat{\sigma}}. \tag{18}$$

The HFV equations in the matrix domain and those in the fault then must be coupled through a discrete version of the coupling equations. For the SLRM with a conforming discretization $(\mathcal{D}, \hat{\mathcal{D}})$ this approximation is quite simple; the bilinear form $cc((\cdot,\cdot),(\cdot,\cdot))$ of (14) is approximated as follows: for $(p,\hat{p})$ and $(v,\hat{v})$ in $\mathcal{V}\times\hat{\mathcal{V}}$,

$$cc\big((p,\hat{p}),(v,\hat{v})\big) \approx \sum_{\hat{K}\in\hat{M}} \frac{\hat{\lambda}_{\boldsymbol{n}}}{2}\big|\hat{K}\big|\,[\![p]\!]_{\hat{K}}\,[\![v]\!]_{\hat{K}} + \sum_{\hat{K}\in\hat{M}} 2\hat{\lambda}_{\boldsymbol{n}}\big|\hat{K}\big|\left(\{\!\{p\}\!\}_{\hat{K}} - \hat{p}_{\hat{K}}\right)\left(\{\!\{v\}\!\}_{\hat{K}} - \hat{v}_{\hat{K}}\right). \tag{19}$$

where the jump and the average term are given by

$$[\![p]\!]_{\hat{K}} = p_{\sigma_{\hat{K},1}} - p_{\sigma_{\hat{K},2}}, \quad \{\!\{p\}\!\}_{\hat{K}} = \frac{p_{\sigma_{\hat{K},1}} + p_{\sigma_{\hat{K},2}}}{2},$$

with $\sigma_{\hat{K},j}$ the face in $\mathcal{E}_{j,\hat{\gamma}}$ coinciding with $\hat{K}$.

For the DLRM, even with a conforming discretization, the fault cells in $\hat{\mathcal{M}}_1$ do not match up with those in $\hat{\mathcal{M}}_2$ and this non matching between the two layers must be taken into account. Here the expression for the bilinear form $cc((\cdot,\cdot),(\cdot,\cdot))$ given in (10) is used. For the first term of (10) we must consider a common refinement of the meshes $\hat{\mathcal{M}}_j$. We let $\hat{\hat{\mathcal{M}}}$ be the smallest common refinement

$$\hat{\hat{\mathcal{M}}} = \{\hat{\hat{K}} = \hat{K}_1 \cap \hat{K}_2 \neq \emptyset \,:\, \hat{K}_j \in \hat{\mathcal{M}}_j\},$$

and the approximation is given by

$$\sum_{\hat{\hat{K}}\in\hat{\hat{\mathcal{M}}}} \hat{\lambda}_{\boldsymbol{n}}|\hat{\hat{K}}|(\hat{p}_{\hat{K}_{\hat{\hat{K}},1}} - \hat{p}_{\hat{K}_{\hat{\hat{K}},2}})(\hat{v}_{\hat{K}_{\hat{\hat{K}},1}} - \hat{v}_{\hat{K}_{\hat{\hat{K}},2}}), \tag{20}$$

where $\hat{K}_{\hat{\hat{K}},j} \in \hat{\mathcal{M}}_j$ is such that $\hat{\hat{K}} = \hat{K}_{\hat{\hat{K}},1} \cap \hat{K}_{\hat{\hat{K}},2}$. The second term of (10), which is not affected by the fact that the discretizations of the two layers of the fault may not coincide, is approximated simply by

$$\sum_j \sum_{\hat{K}_j\in\hat{\mathcal{M}}_j} 2\hat{\lambda}_{\boldsymbol{n}}|\hat{K}_j|(p_{\sigma_{\hat{K}_j}} - \hat{p}_{\hat{K}_j})(v_{\sigma_{\hat{K}_j}} - \hat{v}_{\hat{K}_j}), \tag{21}$$

where $\sigma_{\hat{K}_j}$ is the face in $\mathcal{E}_{\hat{\gamma},j}$ coinciding with $\hat{K}_j$.

## 4.2 Discretization with virtual fault cells

We consider another type of discretization based on a different construction of the fault mesh. This second approach avoids the explicit construction of the tangential operators placing all of the complexity of the approximation on the construction of the fault mesh. We start with a conforming discretization $(\mathcal{D}, \hat{\mathcal{D}})$ as described in the preceding subsection and construct a new discretization $(\mathcal{D}, \widehat{\mathcal{D}})$ consisting only of $N$-dimensional cells. This second method of discretization in fact is made by giving width to the interface cells in the direction normal to the interface and can be seen in some loose sense as the inverse of the process used to obtain the reduced model. We will use the wide hat notation $\widehat{\cdot}$ to denote objects pertaining to the virtual fault domain.

**Definition 3** (Virtual fault cell - SLRM)**.** *Given $\hat{K} \in \hat{\mathcal{M}}$ we construct an $N$-dimensional cell $\widehat{K}$, called a virtual fault cell, by expanding $\hat{K}$ in both directions $\pm\boldsymbol{n}$, normal to the fault:*

$$\widehat{K} = \left\{ \boldsymbol{x} = \hat{\boldsymbol{x}} + \frac{\xi d}{2}\boldsymbol{n} \in \mathbb{R}^N : \hat{\boldsymbol{x}} \in \hat{K}, |\xi| < 1 \right\}.$$

**Definition 4** (Virtual fault cell - DLRM)**.** *Given $\hat{K} \in \hat{\mathcal{M}}_j$ we construct the $N$-dimensional cell $\widehat{K}$, called a virtual fault cell, by expanding $\hat{K}$ in the normal direction but only on one side of the fault, the side toward $\Omega_j$, i.e. in the direction $(-1)^j\boldsymbol{n}$:*

$$\widehat{K} = \left\{ \boldsymbol{x} = \hat{\boldsymbol{x}} + (-1)^j \frac{\xi d}{2}\boldsymbol{n} : \hat{\boldsymbol{x}} \in \hat{K}, 0 \le \xi < 1 \right\}.$$

In Figure 5 we show an example of the construction of virtual cells for both the SLRM and DLRM. We consider the mesh $\widehat{\mathcal{M}}$ for the faults defined to be the collection of all the virtual cells. We will also need a set of faces $\widehat{\mathcal{E}}$ and a set of points $\widehat{\mathcal{P}}$.

**Definition 5** (Discretization of $\hat{\gamma}$ by virtual cells - SLRM)**.** *Given a conforming discretization $(\mathcal{D}, \hat{\mathcal{D}})$ of $(\Omega, \hat{\gamma})$ as defined in Definition 2, the corresponding discretization of $\hat{\gamma}$ by virtual fault cells, is defined to be the triplet $\widehat{\mathcal{D}} := \left(\widehat{\mathcal{M}}, \widehat{\mathcal{E}}, \widehat{\mathcal{P}}\right)$, where $\widehat{\mathcal{M}}$ is the set of virtual fault cells obtained by expanding the cells of $\hat{\mathcal{M}}$, $\widehat{\mathcal{E}}$ is the set of ($(N-1)$-dimensional) faces of cells in $\widehat{\mathcal{M}}$, and $\widehat{\mathcal{P}}$ is the set of points that are the barycentres of elements of $\widehat{\mathcal{M}}$ or of elements of $\widehat{\mathcal{E}}$.*

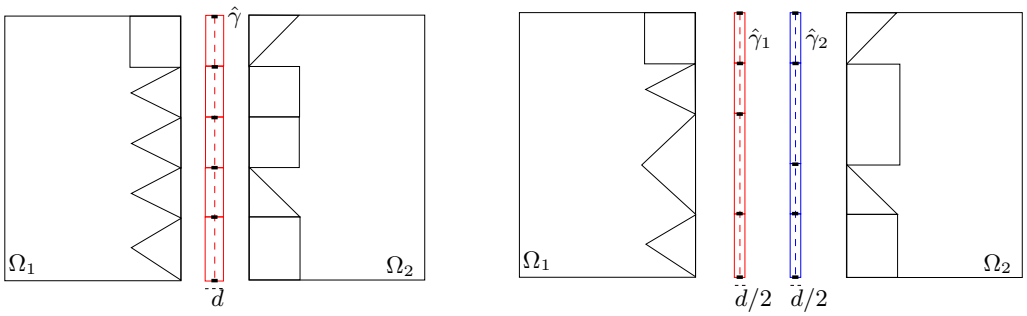
Now we construct the set $\mathcal{M}' = \mathcal{M} \cup \widehat{\mathcal{M}}$ but in which we identify the faces in $\mathcal{E}_{j,\hat{\gamma}}$ with the corresponding faces in $\widehat{\mathcal{E}}$ on the $j^{\text{th}}$ side of $\hat{\gamma}$. In this manner we obtain a set of cells $\mathcal{M}'$ which may be thought of as a mesh for the "virtual domain" $\widehat{\Omega}$ obtained from $\Omega$ by expanding the "flat domain" $\hat{\gamma}$ to obtain an $N$-dimensional fault domain of width $d$. More precisely, since we have assumed that the discretization $(\mathcal{D}, \hat{\mathcal{D}})$ is conforming, each face $\sigma_j \in \mathcal{E}_{j,\hat{\gamma}}$ coincides with a cell $\hat{K} \in \hat{\mathcal{M}}$, that we may denote $\hat{K}_{\sigma_j}$. Then the virtual cell $\widehat{K}_{\sigma_j} \in \widehat{\mathcal{M}}$ obtained by expanding $\hat{K}_{\sigma_j}$ has one face $\sigma_{\widehat{K}_{\sigma_j}}$ parallel to $\hat{K}_{\sigma_j}$ and on the $j^{\text{th}}$ side of $\hat{K}_{\sigma_j}$, and we shall identify this face with $\sigma_j$. There will be only one pressure unknown associated with each face $\sigma_j$; *i.e.* $p_{\sigma_j} = p_{\sigma_{\widehat{K}_{\sigma_j}}}$. Then with $\mathcal{E}'$ and $\mathcal{P}'$ defined in the obvious manner, we may consider the discretization $\mathcal{D}' = (\mathcal{M}', \mathcal{E}', \mathcal{P}')$ as a discretization of the domain

$$\overline{\widehat{\Omega}} := \overline{\Omega_1} \cup \overline{\Omega_2} \cup \overline{\widehat{\gamma}},$$

where $\widehat{\gamma}$ is the interior of the union of the closures of the virtual cells in $\widehat{\mathcal{M}}$. Now we may apply the standard HFV method to the discretization $\mathcal{D}'$ of $\widehat{\Omega}$.

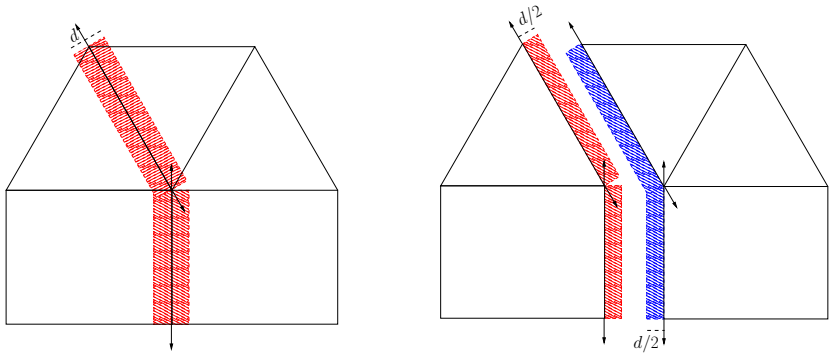
We will show below that, under certain hypotheses, this scheme is equivalent to the scheme defined earlier.

**Remark 1.** *In the general case where the fault segments are not collinear it is still possible to build up the virtual cells, however a more careful description of the pairs of degrees of freedom should be considered. Moreover the virtual cells may overlap each others. In Section 5 we consider faults made of non collinear elements. See Figure 6 for an example of virtual cells for a general mesh.*




(a) SLRM (b) DLRM

Figure 5: Representation of virtual cells, in red, for a general configuration.




(a) SLRM (b) DLRM

Figure 6: Example of construction of virtual cells, for both the SLRM and DLRM, for a general configuration. The arrow in the figure are the outward normals for the tangential part of the fault cells.

### 4.3 Comparison of the two approaches

In this subsection we prove two results that can be useful for the implementation of the proposed method. In particular, we show that for the SLRM, the implementation of the HFV method for the reduced model by the method with virtual cells as described in Subsection 4.2 is equivalent to the implementation with the discretization described in Subsection 4.1 cf. also [32, section 5] where a similar result for the SLRM discretized with a mixed method was used to establish error estimates. For the DLRM we show equivalence of modifications of the two methods obtained by discretizing in the fault with a 2 point flux scheme instead of the HFV method while retaining the HFV method for discretization in the matrix cells of $\mathcal{M}_1$ and $\mathcal{M}_2$ and retaining the discretization given for the coupling conditions.

**Theorem 1** (Discrete equivalence - SLRM)**.** *For a domain $\Omega$ with an interface fault $\hat{\gamma}$ modeled with the SLRM and a conforming discretization $(\mathcal{D}, \hat{\mathcal{D}})$, the numerical solution obtained using the HFV method of Subsection 4.1 with stabilization parameters $\alpha$ and $\hat{\alpha}$ satisfying $\alpha N = 2$ and $\alpha N = 2\hat{\alpha}(N-1)$ is equivalent to that obtained using the HFV method with stabilization parameter $\alpha$ for the associated virtual fault discretization $\mathcal{D}' = (\mathcal{D}, \widehat{\mathcal{D}})$ of the virtual domain $\widehat{\Omega}$ described in Subsection 4.2.*

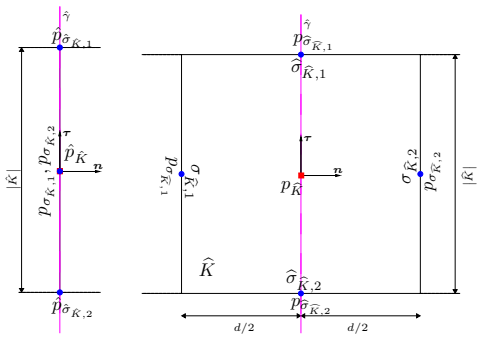
*Proof.* For simplicity we give the proof only in the case in which $N = 2$, the proof in the case $N = 3$ being quite similar. Also for simplicity we assume that $\Lambda_f$ is constant. It is easy to check that there is an obvious correspondence between the unknown values

$$p = ((p_K)_{K\in\mathcal{M}}, (p_\sigma)_{\sigma\in\mathcal{E}}) \text{ and}$$
$$\hat{p} = \big((\hat{p}_{\hat{K}})_{\hat{K}\in\hat{\mathcal{M}}}, (\hat{p}_{\hat{\sigma}})_{\hat{\sigma}\in\hat{\mathcal{E}}}\big)$$

for the standard HFV discretization for the reduced model and those for the discretization with virtual fault cells

$$p' = ((p'_K)_{K\in\mathcal{M}'}, (p'_\sigma)_{\sigma\in\mathcal{E}'})\,;$$

see Figure 7. For the SLRM, the bilinear form




(a) $1D$ (b) $2D$

Figure 7: Notations for a $1D$-cell and a virtual $2D$-cell. The names of the unknowns are chosen along to easily compare the results.

$a\big((\cdot,\cdot),(\cdot,\cdot)\big) + cc\big((\cdot,\cdot),(\cdot,\cdot)\big)$ of (11) is made up of four parts: $a_\Omega(\cdot,\cdot), a_{\hat{\gamma}}(\cdot,\cdot)$ and the two terms of $cc\big((\cdot,\cdot),(\cdot,\cdot)\big)$ as given in (14). For the virtual fault scheme the weak formulation takes the form

$$\begin{aligned} &\text{find } p \in \mathcal{V}_{\widehat{\Omega}} \text{ such that} \\ &a_{\widehat{\Omega}}(p, v) = F(v), \\ &\text{for all } v \in \mathcal{V}_{\widehat{\Omega}}, \end{aligned} \tag{22}$$

where $\mathcal{V}_{\widehat{\Omega}} = H^1_\Gamma(\widehat{\Omega})$ and where

$$a_{\widehat{\Omega}}(p, v) := (\Lambda\nabla p, \nabla v)_{\widehat{\Omega}}\,.$$

To compare the two schemes we first observe that for $p$ and $v$ in $\mathcal{V}_{\widehat{\Omega}}$, we have

$$a_{\widehat{\Omega}}(p, v) = (\Lambda\nabla p, \nabla v)_{\Omega_1\cup\Omega_2} + (\Lambda\nabla p, \nabla v)_{\widehat{\gamma}}\,, \tag{23}$$

where $\widehat{\gamma}$ is the interior of the union of the closures of the virtual cells. Then we compare the approximations of these bilinear forms. As the terms from the form $a_\Omega(\cdot,\cdot)$ are exactly the same as those in the first term in the decomposition of $a_{\widehat{\Omega}}(\cdot,\cdot)$ given in (23), and they are approximated in precisely the same manner, we are left to compare the approximation of $a_{\hat{\gamma}}(\cdot,\cdot) + cc((\cdot,\cdot),(\cdot,\cdot))$ with that of the second term of the decomposition of $a_{\widehat{\Omega}}(\cdot,\cdot)$ given in (23). From (19), we see that the bilinear form $cc\big((\cdot,\cdot),(\cdot,\cdot)\big)$ of (14) is approximated as

follows: for $(p,\hat{p})$ and $(v,\hat{v})$ in $\mathcal{V}\times\hat{\mathcal{V}}$,

$$cc\big((p,\hat{p}),(v,\hat{v})\big) \approx \sum_{\hat{K}\in\hat{M}} \frac{\hat{\lambda}_{\boldsymbol{n}}}{2}\big|\hat{K}\big| \left[\!\left[p\right]\!\right]_{\hat{K}} \left[\!\left[v\right]\!\right]_{\hat{K}} + \sum_{\hat{K}\in\hat{M}} 2\hat{\lambda}_{\boldsymbol{n}}\big|\hat{K}\big| \left(\{\!\{p\}\!\}_{\hat{K}} - \hat{p}_{\hat{K}}\right)\left(\{\!\{v\}\!\}_{\hat{K}} - \hat{v}_{\hat{K}}\right). \tag{24}$$

From (16)-(18), we calculate that the bilinear form $a_{\hat{\gamma}}(\cdot,\cdot)$ of (13), corresponding to the tangential flow equation (12b), is approximated as follows: for $\hat{p}$ and $\hat{v}$ in $\hat{\mathcal{V}}$,

$$\begin{aligned} a_{\hat{\gamma}}(\hat{p},\hat{v}) &= \sum_{\hat{K}\in\hat{\mathcal{M}}} \int_{\hat{K}} 2\hat{\lambda}\nabla_{\boldsymbol{\tau}}\hat{p}\cdot\nabla_{\boldsymbol{\tau}}\hat{v}\mathrm{d}\hat{x} \\ &\approx \sum_{\hat{K}\in\hat{\mathcal{M}}} \int_{\hat{K}} 2\hat{\lambda}\hat{\nabla}_{\mathcal{D}}\,\hat{p}\cdot\hat{\nabla}_{\mathcal{D}}\,\hat{v}\mathrm{d}\hat{x} \\ &= \sum_{\hat{K}\in\hat{\mathcal{M}}} 2\hat{\lambda}\big|\hat{K}\big|\hat{\nabla}_{\hat{K}}\hat{p}\cdot\hat{\nabla}_{\hat{K}}\hat{v} \\ &\quad +2\sum_{\hat{K}\in\hat{\mathcal{M}}} \hat{\lambda}\big|\hat{K}\big|\sum_{j=1}^{2} R_{\hat{K},\hat{\sigma}_{\hat{K},j}}\hat{p}R_{\hat{K},\hat{\sigma}_{\hat{K},j}}\hat{v}, \end{aligned}$$

where $\hat{\sigma}_{\hat{K},1}$ and $\hat{\sigma}_{\hat{K},2}$ are the two faces (*i.e.* vertices) of $\hat{K}$, which we suppose are numbered such that the vector pointing from $\hat{\sigma}_{\hat{K},2}$ toward $\hat{\sigma}_{\hat{K},1}$ is oriented in the same direction as $\boldsymbol{\tau}$, so that the second summation in the last term is over the two cones (*i.e.* half segments) of $\hat{K}$. The cell gradient may be written

$$\hat{\nabla}_{\hat{K}}\hat{p} = \frac{1}{\big|\hat{K}\big|}\delta_{\hat{K}}(\hat{p}_{\hat{\sigma}})\boldsymbol{\tau},$$

where we have written $\delta_{\hat{K}}(\hat{p}_{\hat{\sigma}})$ for $\hat{p}_{\hat{\sigma}_{\hat{K},1}} - \hat{p}_{\hat{\sigma}_{\hat{K},2}}$, while the stabilization term in the cone $D_{\hat{K},\hat{\sigma}_{\hat{K},j}}$ is

$$R_{\hat{K},\hat{\sigma}_{\hat{K},j}}\hat{p} = (-1)^j \frac{\hat{\beta}}{\big|\hat{K}\big|/2}\left(\mu_{\hat{K}}(\hat{p}_{\hat{\sigma}}) - \hat{p}_{\hat{K}}\right),$$

where we have denoted by $\mu_{\hat{K}}(\hat{p}_{\hat{\sigma}})$ the average value $(\hat{p}_{\hat{\sigma}_{\hat{K},1}} + \hat{p}_{\hat{\sigma}_{\hat{K},2}})/2$ . So we may now write the approximation for the bilinear form $a_{\hat{\gamma}}(\cdot,\cdot)$, as follows:

$$a_{\hat{\gamma}}(\hat{p},\hat{v}) \approx \sum_{\hat{K}\in\hat{\mathcal{M}}} \frac{2\hat{\lambda}}{\big|\hat{K}\big|}\delta_{\hat{K}}(\hat{p}_{\hat{\sigma}})\delta_{\hat{K}}(\hat{v}_{\hat{\sigma}}) + \sum_{\hat{K}\in\hat{\mathcal{M}}} \frac{8\hat{\lambda}\hat{\beta}^2}{\big|\hat{K}\big|}\left(\mu_{\hat{K}}(\hat{p}_{\hat{\sigma}}) - \hat{p}_{\hat{K}}\right)\left(\mu_{\hat{K}}(\hat{v}_{\hat{\sigma}}) - \hat{v}_{\hat{K}}\right), \tag{25}$$

with $\hat{\beta} = \sqrt{\hat{\alpha}(N-1)}$.

We next need to make explicit the terms in the approximation of the second term in the decomposition given in (23) of $a_{\widehat{\Omega}}(\cdot,\cdot)$ which we then split into tangential and normal components: for $p$ and $v$ in $\mathcal{V}_{\widehat{\Omega}}$,

$$\begin{aligned} (\Lambda\nabla p,\nabla v)_{\widehat{\gamma}} &\approx \sum_{\widehat{K}\in\widehat{\mathcal{M}}} \int_{\widehat{K}} \nabla_{\mathcal{D}}\,p\cdot\Lambda\nabla_{\mathcal{D}}\,v\mathrm{d}\boldsymbol{x} \\ &= \sum_{\widehat{K}\in\widehat{\mathcal{M}}} \int_{\widehat{K}} \boldsymbol{N}\nabla_{\mathcal{D}}\,p\cdot\Lambda\boldsymbol{N}\nabla_{\mathcal{D}}\,v\mathrm{d}\boldsymbol{x} \\ &\quad + \sum_{\widehat{K}\in\widehat{\mathcal{M}}} \int_{\widehat{K}} \boldsymbol{T}\nabla_{\mathcal{D}}\,p\cdot\Lambda\boldsymbol{T}\nabla_{\mathcal{D}}\,v\mathrm{d}\boldsymbol{x}. \end{aligned}$$

For $\widehat{K}\in\widehat{\mathcal{M}}$ and $\sigma_{\widehat{K},j}$ the face of $\widehat{K}$ identified with a face in $\mathcal{E}_{j,\hat{\gamma}}$ and $\widehat{\sigma}_{\widehat{K},1}$ and $\widehat{\sigma}_{\widehat{K},2}$ the remaining two faces of $\widehat{K}$ numbered such that $\boldsymbol{\tau}$ points from the midpoint of $\widehat{\sigma}_{\widehat{K},2}$ toward that of $\widehat{\sigma}_{\widehat{K},1}$, (see Figure 7) the cell gradient maybe written as follows:

$$\nabla_{\widehat{K}}p = -\frac{1}{d}(p_{\sigma_{\widehat{K},1}} - p_{\sigma_{\widehat{K},2}})\boldsymbol{n} + \frac{1}{\big|\widehat{K}\big|}(p_{\widehat{\sigma}_{\widehat{K},1}} - p_{\widehat{\sigma}_{\widehat{K},2}})\boldsymbol{\tau},$$

where we recall that $\widehat{K}$ is a rectangle with $\big|\widehat{K}\big| = d\big|\hat{K}\big|$, while the four stabilization terms are

$$\begin{aligned} R_{\widehat{K},\sigma_{\widehat{K},j}}p\boldsymbol{n}_{\widehat{K},\sigma_{\widehat{K},j}} &= (-1)^j\frac{2\beta}{d}\left(\mu_{\widehat{K}}(p_\sigma) - p_{\widehat{K}}\right)\boldsymbol{n} \\ R_{\widehat{K},\widehat{\sigma}_{\widehat{K},j}}p\boldsymbol{n}_{\widehat{K},\widehat{\sigma}_{\widehat{K},j}} &= (-1)^{j+1}\frac{2\beta}{\big|\widehat{K}\big|}\left(\mu_{\widehat{K}}(p_{\widehat{\sigma}}) - p_{\widehat{K}}\right)\boldsymbol{\tau}, \end{aligned}$$

with the average terms $\mu_{\widehat{K}}(p_\sigma) = (p_{\sigma_{\widehat{K},1}} + p_{\sigma_{\widehat{K},2}})/2$ and $\mu_{\widehat{K}}(p_{\widehat{\sigma}}) = (p_{\widehat{\sigma}_{\widehat{K},1}} + p_{\widehat{\sigma}_{\widehat{K},2}})/2$. The

contribution from the normal part of the discrete term is thus

$$\begin{aligned}&\sum_{\widehat{K}\in\widehat{\mathcal{M}}}\int_{\widehat{K}}\boldsymbol{N}\nabla_{\mathcal{D}}\,p\cdot\Lambda\boldsymbol{N}\nabla_{\mathcal{D}}\,v\mathrm{d}\boldsymbol{x}\\&=\sum_{\widehat{K}\in\widehat{\mathcal{M}}}\frac{\hat{\lambda}_{\boldsymbol{n}}}{2}\big|\hat{K}\big|\delta_{\widehat{K}}(p_\sigma)\delta_{\widehat{K}}(v_\sigma)\\&+\sum_{\widehat{K}\in\widehat{\mathcal{M}}}\hat{\lambda}_{\boldsymbol{n}}\big|\hat{K}\big|\beta^2\big(\mu_{\widehat{K}}(p_\sigma)-p_{\widehat{K}}\big)\big(\mu_{\widehat{K}}(v_\sigma)-v_{\widehat{K}}\big),\end{aligned}\tag{26}$$

while that from the tangential part is

$$\begin{aligned}&\sum_{\widehat{K}\in\widehat{\mathcal{M}}}\int_{\widehat{K}}\boldsymbol{T}\nabla_{\mathcal{D}}\,p\cdot\Lambda\boldsymbol{T}\nabla_{\mathcal{D}}\,v\mathrm{d}\boldsymbol{x}\\&=\sum_{\widehat{K}\in\widehat{\mathcal{M}}}\frac{2\hat{\lambda}}{\big|\hat{K}\big|}\delta_{\widehat{K}}(p_{\hat{\sigma}})\delta_{\widehat{K}}(v_{\hat{\sigma}})\\&+\sum_{\widehat{K}\in\widehat{\mathcal{M}}}\frac{4\hat{\lambda}\beta^2}{\big|\hat{K}\big|}\big(\mu_{\widehat{K}}(p_{\hat{\sigma}})-p_{\widehat{K}}\big)\big(\mu_{\widehat{K}}(v_{\hat{\sigma}})-v_{\widehat{K}}\big),\end{aligned}\tag{27}$$

with $\delta_{\widehat{K}}(p_\sigma) = p_{\sigma_{\widehat{K},1}} - p_{\sigma_{\widehat{K},2}}$ and $\delta_{\widehat{K}}(p_{\hat{\sigma}}) = p_{\hat{\sigma}_{\widehat{K},1}} - p_{\hat{\sigma}_{\widehat{K},2}}$, and $\beta = \sqrt{\alpha N}$. Now identifying for each $\hat{K}\in\hat{\mathcal{M}}$, the unknowns $\hat{p}_{\hat{K}}$, $\hat{p}_{\hat{\sigma}_{\hat{K},1}}$, $\hat{p}_{\hat{\sigma}_{\hat{K},2}}$, $p_{\sigma_{\hat{K},1}}$ and $p_{\sigma_{\hat{K},2}}$, respectively, of the HFV discretization of the SLRM with the unknowns $p_{\widehat{K}}, p_{\hat{\sigma}_{\widehat{K},1}}, p_{\hat{\sigma}_{\widehat{K},2}}, p_{\sigma_{\widehat{K},1}}$ and $p_{\sigma_{\widehat{K},2}}$, respectively of the HFV discretization of $\widehat{\Omega}$ using virtual elements we have that equation (26) is equivalent to (24) if $\beta^2 = 2$, while equation (27) is equivalent to (25) provided that $2\hat{\beta}^2 = \beta^2$. □

We turn our attention now to a comparison of the the two discretization techniques for the DLRM for a domain $\Omega$ with interface fault $\hat{\gamma} = \hat{\gamma}_1 = \hat{\gamma}_2$. We suppose that we have a conforming discretization $(\mathcal{D}, \hat{\mathcal{D}})$, and recall that this does not imply that $\hat{\mathcal{M}}_1$ coincides with $\hat{\mathcal{M}}_2$. We point out though that in the case that $\hat{\mathcal{M}}_1$ and $\hat{\mathcal{M}}_2$ do coincide the demonstration of Theorem 1 extends immediately to show that the discretization with virtual ($N$-dimensional) fault cells and that with interface ($(N-1)$-dimensional) cells for the fault are equivalent with the appropriate conditions on $\beta$ and $\hat{\beta}$. However in the general case (when the grids $\hat{\mathcal{M}}_1$ and $\hat{\mathcal{M}}_2$ in the fault are non matching) such an equivalence no longer holds as tangential terms of the discrete gradient are involved in the approximation of the coupling conditions. In the following theorem however we do obtain an equivalence when the classical two-point flux scheme is used for the problem inside the fault (while retaining the HFV method in the matrix domains).

Before stating the equivalence theorem for the DLRM we give a more precise description of the modification of each scheme that is used in the theorem. For the discretization using $(N-1)$-dimensional cells in the fault the modifications are as follows:

- for the discretization of the bilinear form $a_\Omega(\cdot,\cdot)$ there is no change as the HFV method is still used.
- for the discretization of $a_{\hat{\gamma}}(\cdot,\cdot)$ the HFV method is replaced by the two point flux method: there are no pressure unknowns on the faces $\hat{\sigma}_{\hat{K},j}$ of the cells $\hat{K}\in\hat{\mathcal{M}}$.
- for the discretization of $cc\big((\cdot,\cdot),(\cdot,\cdot)\big)$ there is no change.

For the discretization using virtual ($N$-dimensional) cells in the fault we have

- for the discretization of the first term in the decomposition (23) of $a_{\widehat{\Omega}}(\cdot,\cdot)$ there is no change: the HFV method is used.
- for the discretization of the second term in the decomposition (23) of $a_{\widehat{\Omega}}(\cdot,\cdot)$ the two point flux method is used with a minor modification:
  - for the tangential component the standard two-point flux method is used. There are no pressure unknowns associated with the faces $\widehat{\sigma}_{\widehat{K},j}$ of $\widehat{K}_j\in\widehat{\mathcal{M}}_j$ that lie in the interior of $\widehat{\gamma}$.
  - for the normal component, for a cell $\widehat{K}_j\in\widehat{\mathcal{M}}_j$, as the HFV method has been used in the neighboring cell $K_j\in\mathcal{M}_j$ there is a pressure value

available on the the face $\sigma_{\widehat{K}_j}$ common to the virtual cell $\widehat{K}_j$ and to the cell $K_j$. The value $p_{\sigma_{\widehat{K}_j}}$ together with the value $p_{\widehat{K}_j}$ is used to approximate the normal component of the gradient of $p$ in $\widehat{K}_j$ (instead of the value $p_{K_j}$).

The following result shows the equivalence when a two-point flux scheme is considered to approximate the tangential component of the second term of (23), but would also be the case if we were using the HFV method, provided or course that $2\hat{\beta}^2 = \beta^2$. The proof is given in the simple case of planar faults.

**Theorem 2** (Two-points discrete equivalence - DLRM)**.** *Suppose $\Omega$ is a domain with an interface fault $\hat{\gamma}$ modeled with the DLRM and that $(\mathcal{D}, \hat{\mathcal{D}})$ is a conforming discretization of $(\Omega, \hat{\gamma})$. The numerical solution obtained using the HFV method of Subsection 4.1 but a two-point scheme as described above for the fault is equivalent to that obtained using the HFV method for the associated virtual fault discretization $\mathcal{D}' = (\mathcal{D}, \widehat{\mathcal{D}})$ of the virtual domain $\widehat{\Omega}$ described in Subsection 4.2 with the modification for the virtual cells described above.*

*Proof.* Again for simplicity we assume $N = 2$ and that $\Lambda_f$ is constant. As in the proof of Theorem 1 it is sufficient to compare the terms coming from the bilinear forms $cc\big((\cdot,\cdot),(\cdot,\cdot)\big)$ and $a_{\hat{\gamma}}(\cdot,\cdot)$, *i.e.* from the coupling terms and those associated with flow in the fault, with the terms associated with the second term in (23). It is also clear that the terms in the discretization of $a_{\hat{\gamma}}(\cdot,\cdot)$ correspond precisely to those in the tangential component of the discretization of the second term of (23).

So we have left to compare the terms associated with the discretization of $cc\big((\cdot,\cdot),(\cdot,\cdot)\big)$ with those associated with the normal component of the discretization of the second term of (23). From (10) and the approximations given in (20) and (21) we have the approximation of $cc\big((p,\hat{p}),(v,\hat{v})\big)$ is given as follows:

$$\sum_j \sum_{\hat{K}_j \in \hat{\mathcal{M}}_j} 2\hat{\lambda}_{\boldsymbol{n}} |\hat{K}_j| (p_{\sigma_{\hat{K}_j}} - \hat{p}_{\hat{K}_j})(v_{\sigma_{\hat{K}_j}} - \hat{v}_{\hat{K}_j}) \quad (28)$$

$$+ \sum_{\hat{\hat{K}} \in \hat{\hat{\mathcal{M}}}} \hat{\lambda}_{\boldsymbol{n}} |\hat{\hat{K}}| (\hat{p}_{\hat{K}_{\hat{\hat{K}},1}} - \hat{p}_{\hat{K}_{\hat{\hat{K}},2}})(\hat{v}_{\hat{K}_{\hat{\hat{K}},1}} - \hat{v}_{\hat{K}_{\hat{\hat{K}},2}}), \quad (29)$$

where as in (20), $\hat{\hat{\mathcal{M}}}$ is the smallest common refinement of $\hat{\mathcal{M}}_1$ and $\hat{\mathcal{M}}_2$, and for $\hat{\hat{K}} \in \hat{\hat{\mathcal{M}}}$, $\hat{K}_{\hat{\hat{K}},j} \in \hat{\mathcal{M}}_j$ is such that $\hat{K}_{\hat{\hat{K}},1} \cap \hat{K}_{\hat{\hat{K}},2} = \hat{\hat{K}}$.

The normal component of the second term of (23) is $(\lambda_{f,\boldsymbol{n}} \dfrac{\partial p}{\partial \boldsymbol{n}}, \dfrac{\partial v}{\partial \boldsymbol{n}})_{\hat{\gamma}}$ and is approximated by

$$\sum_j \sum_{\widehat{K}_j \in \widehat{\mathcal{M}}_j} 2\hat{\lambda}_{\boldsymbol{n}} |\hat{K}_j| (p_{\sigma_{\widehat{K}_j}} - p_{\widehat{K}_j})(v_{\sigma_{\widehat{K}_j}} - v_{\widehat{K}_j}) \quad (30)$$

$$+ \sum_{\widehat{\hat{K}} \in \widehat{\hat{\mathcal{M}}}} \hat{\lambda}_{\boldsymbol{n}} |\hat{\hat{K}}| (p_{\widehat{K}_{\hat{\hat{K}},2}} - p_{\widehat{K}_{\hat{\hat{K}},1}})(v_{\widehat{K}_{\hat{\hat{K}},2}} - v_{\widehat{K}_{\hat{\hat{K}},1}}), \quad (31)$$

where we have used the fact that for $\widehat{K}_j \in \widehat{\mathcal{M}}_j$,

$$\lambda_{f,\boldsymbol{n}} |\widehat{K}_j| = \lambda_{f,\boldsymbol{n}} \frac{d|\hat{K}_j|}{4} = 2\hat{\lambda}_{\boldsymbol{n}} \left(\frac{d}{4}\right)^2 |\hat{K}_j|,$$

and similarly that if $\widehat{\hat{K}} \in \widehat{\hat{\mathcal{M}}}$, then

$$\lambda_{f,\boldsymbol{n}} |\widehat{\hat{K}}| = \lambda_{f,\boldsymbol{n}} \frac{d|\hat{\hat{K}}|}{2} = \hat{\lambda}_{\boldsymbol{n}} \left(\frac{d}{2}\right)^2 |\hat{\hat{K}}|.$$

Now identifying for each $\hat{K}_j \in \hat{\mathcal{M}}_j$, the unknowns $\hat{p}_{\hat{K}_j}$ and $p_{\sigma_{\hat{K}_j}}$, respectively, of the discretization of the DLRM using $(N-1)$-dimensional cells in the fault with the unknowns $p_{\widehat{K}_j}$ and $p_{\sigma_{\widehat{K}_j}}$, respectively, of the discretization of the DLRM using virtual elements in the fault we have that expression (30) is equivalent to (28) while expression (31) is equivalent to (29). □

**Remark 2.** *Theorem 2 shows that the straightforward discretization of the DLRM is similar to a two-point flux approximation of the normal fluxes in the virtual fault cell approach. While this is satisfactory for the fluxes between the fault and its adjacent domain, it is not accurate enough for the fluxes between the two sides of the fault where the grids do not match. Therefore, in the following, we shall only consider the virtual cell approach for which an accurate approximation of the non matching terms is obtained with the HFV scheme.*

# 5 Numerical experiments

In the three following subsections we present several numerical experiments to validate and assess the proposed double-layer reduced model discretized by the hybrid finite volume scheme. The first subsection is devoted to academic tests for an homogeneous porous medium divided into two subdomains by a single fault while the second section considers instead a layered heterogeneous medium outside the fault. For these two academic tests we use a direct method to solve the linear systems. The third section present a realistic test. In all experiments we consider a stabilization parameter $\alpha = 1$.

## 5.1 Model validity: homogeneous case

We consider the domain $\Omega = (0, 100)^2$, with a vertical fault of thickness $d = 2$ running along the middle of $\Omega$: $\hat{\gamma} = \left\{(x, y) \in \mathbb{R}^2 : x = 50\right\}$. See Figure 8a. We assume Dirichlet boundary conditions for

$$\Gamma_{D,1} = \left\{(x, y) \in \mathbb{R}^2 : y = 100 \text{ and } x < 20\right\}$$
$$\Gamma_{D,2} = \left\{(x, y) \in \mathbb{R}^2 : y = 0 \text{ and } x > 80\right\}$$

with data $p = 1$ and homogeneous Neumann boundary conditions for the rest of the boundary. For the fault we impose homogeneous Neumann boundary conditions. We set a source term in the regions

$$\Omega_{q,1} = \{(x, y) \in (0, 2) \times (0, 4)\}$$
$$\Omega_{q,2} = \left\{(x, y) \in (98, 100)^2\right\}$$

equal to $10^{-2}$, for $\Omega_{q,1}$ and $-10^{-2}$ for $\Omega_{q,2}$.

We consider a coarse mesh where the reduced model is used and a fine mesh corresponding to a fine 2-D discretization of a region including the fault is used. In the latter method the fault is discretized with six elements in the normal direction to the fault. See Figures 8b, 8c. One should note that for the reduced model the subdomain meshes do not match. We introduce the relative error between the solution $p_{\text{coarse}}$ obtained with the reduced model and a coarse grid and the full 2-D model solution $p_{\text{fine}}$, that obtained with a fine 2-D discretization of the fault, as an indicator of the validity of the reduced model. For a given cell $K \in \mathcal{M}$ we have

$$err(K) := \frac{\|\Pi p_{\text{fine}} - p_{\text{coarse}}\|_{L^2(K)}}{\|\Pi p_{\text{fine}}\|_{L^2(K)}}, \qquad (32)$$

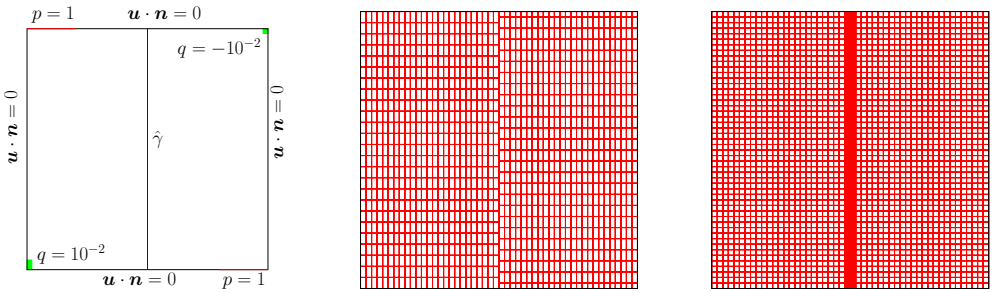
with $\mathcal{M}$ the coarse mesh and $\Pi p_{\text{fine}}$ the interpolation of $p_{\text{fine}}$ on the coarse mesh $\mathcal{M}$, setting up the problem such that the pressure field is not zero.

We consider three test cases corresponding to different permeabilities in the fault while maintaining the identity matrix for the permeability tensor in $\Omega$.

**Barrier** We choose as the permeability in the fault $\Lambda_f = \text{diag}\left\{10^{-2}, 1\right\}$. In Figure 9 we show the solutions obtained with the reduced model, Figure 9a, with the full 2-D model on a refined mesh, Figure 9b, and the error between them $err(K)$ given by equation (32), Figure 9c. We can observe that the largest part of the error is concentrated close to the fault. This is reasonable since the solution presents a steep gradient of the pressure across the fault, as we can see in Figures 9b and 9a. However a little far away from the fault the error is much smaller. The error in all the domain is of the order $\mathcal{O}\left(10^{-2}\right)$, confirming a good approximation in this case.

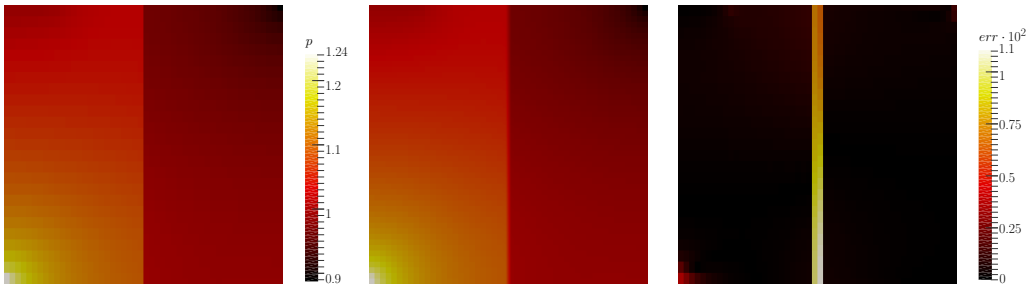
**Channel** We chose as the permeability in the fault $\Lambda_f = \text{diag}\left\{1, 10^2\right\}$. Figure 10 shows the solutions obtained with the reduced model, Figure 10a, with the full 2-D model on a refined mesh, Figure 10b, and the error between them, Figure 10c. We observe that since the solution is smoother the error is spread over the whole domain and not only closed to the fault. For this problem the error is half that of the previous case and is concentrated in the left part of the domain, since there the source term is larger. The solution is qualitatively the same.

**Fully immersed** We chose as the permeability in the fault $\Lambda_f = \text{diag}\left\{10^{-2}, 10^2\right\}$ if $25 \leq y \leq 75$ and $\Lambda_f$ equal to the identity matrix otherwise, like in the subdomains. Figure 11 shows the solutions obtained with the



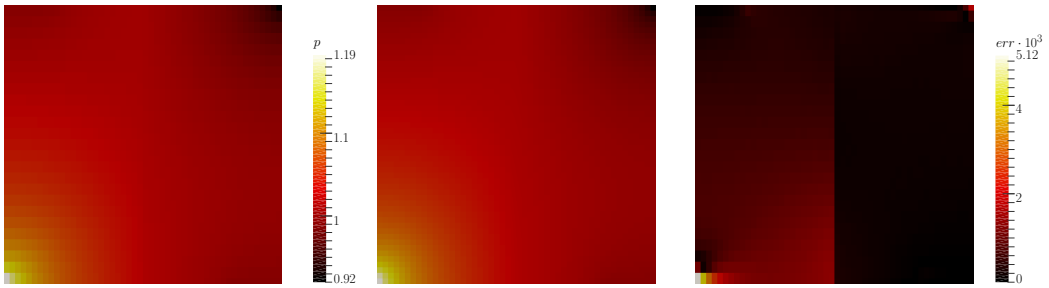

(a) Computational domain. (b) Coarse mesh. (c) Fine mesh.

Figure 8: Homogeneous academic case: (a) computational domain with some of the data for the problem and meshes. The coarse mesh (b) for the reduced model has 1275 hexahedra outside the fault and 51 elements in the fault, while the fine mesh (c) corresponding to a fine 2-D discretization of the fault has 34000 hexahedra.




(a) With the *RM*. (b) Without the *RM*. (c) Model error.

Figure 9: Barrier case: Model error between the reduced model solution on the coarse mesh (Figure 8b) and the full 2-D model solution on the fine mesh (Figure 8c).




(a) With the *RM*. (b) Without the *RM*. (c) Model error.

Figure 10: Channel case: Model error between the reduced model solution on the coarse mesh (Figure 8b) and the full 2-D model solution on the fine mesh (Figure 8c).

reduced model, Figure 11a, with the full 2-D model on a refined mesh, Figure 11b. The behaviour of the error is a combination of the two previous cases. In fact the larger error is concentrated close to the fault and decays away from it. Around the two extremities the error behaves like in the last test case. The error is however of the same magnitude as for the first test case.

## 5.2 Model validity: heterogeneous problem

The following test case is inspired by the last example in [18]. We consider a problem with an heterogeneous porous medium composed by several layers and a fault in its middle. The domain and fault are

$$\Omega = (0, 100)^2 \text{ and } \hat{\gamma} = \left\{(x, y) \in \mathbb{R}^2 : x = 50\right\}$$

with fault thickness $d = 2.5$. We impose a zero source term and for pressure boundary conditions $p = 1.5$ on the top, and $p = 1$ on the bottom. Moreover on the left and on the right we impose a no flow boundary condition. The layers of the porous medium are defined as

$$\Omega_l = \left\{(x, y) \in \mathbb{R}^2 : y \in I_l \text{ and } x < 50\right\}$$
$$\Omega_r = \left\{(x, y) \in \mathbb{R}^2 : y \in I_r \text{ and } x > 50\right\},$$

where the intervals are defined as

$$I_l = [25, 50] \cup [75, 100] \quad \text{and}$$
$$I_r = [12.5, 37.5] \cup [62.5, 87.5].$$

A sketch of the computational domain is given in Figure 12a. The permeability for the two layers are

$$\Lambda_l = \text{diag}\left\{10^{-3}, 10^{-3}\right\} \text{ in } \Omega_l,$$
$$\Lambda_r = \text{diag}\left\{10^{-2}, 10^{-2}\right\} \text{ in } \Omega_r$$

and $\Lambda = \boldsymbol{I}$ in $\Omega \setminus (\Omega_l \cup \Omega_r)$. Also Figure 12a shows two meshes, a non conforming coarse mesh which is used with the reduced model and a fine mesh corresponding to a fine 2-D discretization of the fault which is used for the full 2-D model.

For the permeability in the fault we introduce the parameter $\zeta \in \mathbb{R}^+$ which is the ratio of the permeability in each layer of the fault to the permeability of the closer cell in the porous medium.

In Figure 13 we present the solutions for the reduced model with the coarse mesh shown in Figure 12b and for the full 2-D model with the fine mesh shown in Figure 12c, for $\zeta = 10^{-2}$ and $\zeta = 10^4$. For the case of a small value of $\zeta$, *i.e.* the fault behaves as a barrier, we can see that the two solutions are similar qualitatively. When the fault behaves like a channel, *i.e.* $\zeta = 10^4$, we observe that all the small scales are lost near the fault and they are "homogenized" in a bigger cell. Anyway the model error is still small in this case.

We performed some experiments varying $\zeta$ from $10^{-6}$ up to $10^{10}$. We computed the error (32) for each value of $\zeta$ and we plotted the results in Figure 14. We can see that the maximum of the error is very small for each value of $\zeta$, even if we have an oscillation close to $\zeta = 10^{-1}$. Moreover we notice two different plateaus for $\zeta$ smaller than $10^{-5}$ and bigger than $10^5$. We notice also that we commit at most an error lower than the 7‰, conforming that the method is quite robust despite the fact that the mesh in this test is really coarse.

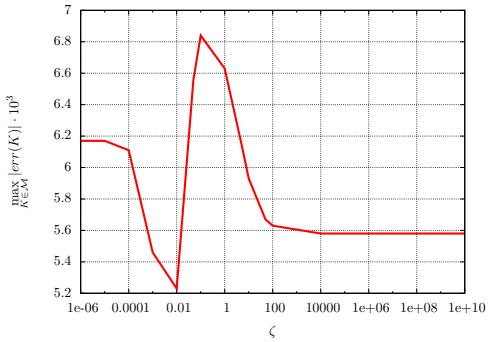
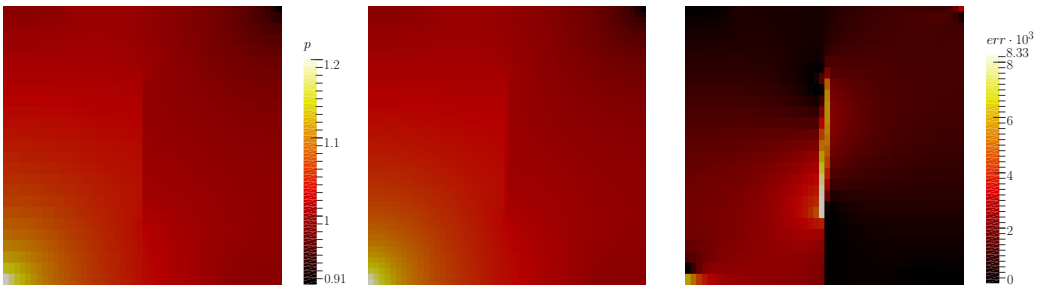



Figure 14: Maximum of model error as a function of $\zeta$.

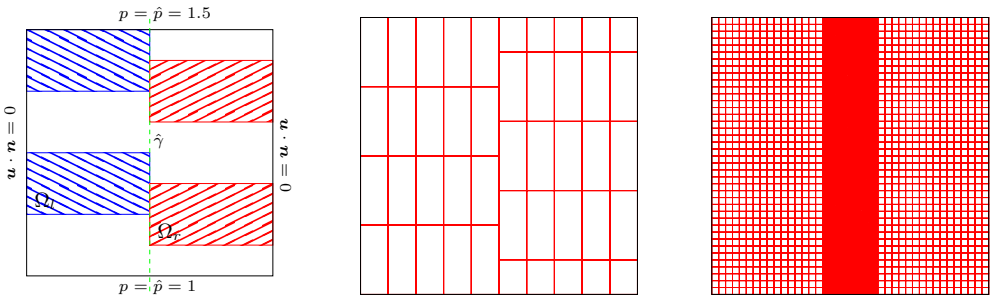
## 5.3 Realistic experiment

We finally consider a problem in a realistic setting. We consider the porous medium depicted in Figure 15a with a T-shape fault presented in Figure 15b and 15c. From these figures we



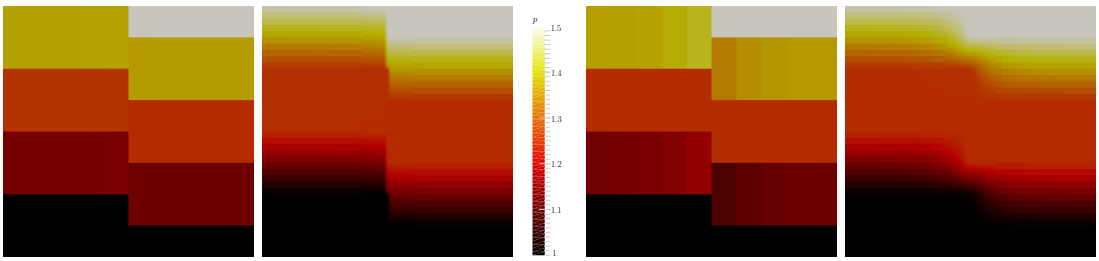

(a) With the *RM*. (b) Without the *RM*. (c) Model error.

Figure 11: Fully immersed case: Model error between the reduced model solution on the coarse mesh (Figure 8b) and the full 2-D model solution on the fine mesh (Figure 8c).




(a) Computational domain. (b) Coarse mesh. (c) Fine mesh.

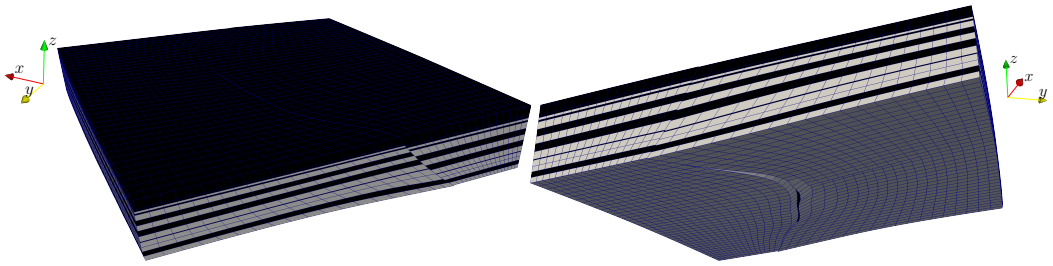
Figure 12: Heterogeneous academic case: (a) computational domain with some of the data and meshes. The coarse mesh (b) for the reduced model has 45 hexahedra outside the fault and 9 elements in the fault, while the fine mesh (c) corresponding to a fine 2-D discretization of the fault has 6400 hexahedra. In blue is depicted $\Omega_l$ and in red is depicted $\Omega_r$.



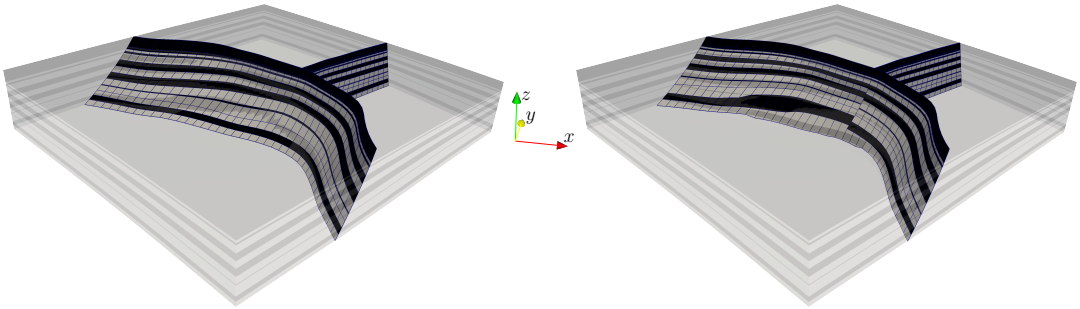

(a) With the RM. (b) Without the RM. (c) With the RM. (d) Without the RM.

$\zeta = 10^{-2}$ $\zeta = 10^{4}$

Figure 13: Heterogeneous academic case: reduced model solutions on the coarse mesh (Figure 12b) and the full 2-D model solutions on the fine mesh (Figure 12c) for two values of $\zeta$.




(a) Different views of the computational domain.




(b) Discretization of the first layer of the faults.

(c) Discretization of the second layer of the faults.

Figure 15: Representation of the domain and the fault grid for both layers. We can notice that the discretization is non-matching and we have a geometrical non-conformity. The colour represents the different homogeneous strata.

can see that the problem exhibits a geometrical non-conformity close to the fault. Unlike in the previous experiments, the faults here are not planar surfaces. This situation produces additional difficulties. Indeed, the two sides of a fault are non-matching, *i.e.* their topological structure differs, but also their geometric realization differ as they can have gaps in between each other due to the discretization. In particular, due to a precedent deposition and movement of the sedimentary layers, because of the fault, we have a different data distribution on the two sides of the fault. We can however use the DLRM using appropriate projections to write the coupling conditions between the two sides of the fault. Moreover, some faces of the fault have only partial contact or even no contact with the other side of the fault. These faces or parts of faces are considered as boundary faces.

We have the following bounds for the computational domain $\Omega \subset (-1.37, 1.34) \cdot 10^4 m \times (-25.6, 1.73) \cdot 10^3 m \times (-4.11 \cdot 10^3, -75.2) m$ and a fault of thickness $d = 50m$. We denote by $\partial\Omega^{\text{top}}$ the top part of the boundary, by $\partial\Omega^{\text{bott}}$ the bottom part of the boundary and by

$$\partial\Omega^{\text{rem}} = \partial\Omega \setminus (\partial\Omega^{\text{top}} \cup \partial\Omega^{\text{bott}})$$

the rest of the boundary. Given $t^*$ and $T$ the initial and final times, we calculate $p$ such that

$$\begin{aligned}
c\Phi \frac{\partial p}{\partial t} &= \nabla \cdot \frac{\Lambda}{\mu} \nabla p && \text{in } \Omega \times (t^*, T), \\
\Lambda \nabla p \cdot \boldsymbol{n} &= 0 && \text{on } \partial\Omega^{\text{rem}} \times (t^*, T), \\
p &= 0 && \text{on } \partial\Omega^{\text{top}} \times (t^*, T), \\
p &= p_0 && \text{in } \Omega \times \{t^*\},
\end{aligned}$$

where $\mu = 3.1 \cdot 10^4 Pa \cdot s$ is the dynamic viscosity, $c$ is the compressibility and $\Phi$ the porosity. Considering Figure 15a, we impose $c\Phi = 0.2 \cdot 10^{-4} Pa^{-1}$ in each of the black layer while $c\Phi = 10^{-4} Pa^{-1}$ in each of the white layer. The initial and final times are $t^* = 0y$ and $T = 2My$ respectively. The initial solution $p_0$ is the stationary solution of

$$\begin{aligned}
-\nabla \cdot \frac{\Lambda}{\mu} \nabla p_0 &= 0 && \text{in } \Omega, \\
\Lambda \nabla p_0 \cdot \boldsymbol{n} &= 0 && \text{on } \partial\Omega^{\text{rem}}, \\
\Lambda \nabla p_0 \cdot \boldsymbol{n} &= 0 && \text{on } \partial\Omega^{\text{bott}}, \\
p_0 &= 0 && \text{on } \partial\Omega^{\text{top}}, \\
p_0 &= 20 && \text{on } \partial\Omega^{\text{bott}}.
\end{aligned}$$

For the computation of $p_0$ we consider the permeability in the fault cells equal to that of the surrounding domain cell, while for the bottom boundary condition of the fault we impose a zero flow condition. We use an implicit Euler scheme for the time discretization. The number of domain cells is 19152, while the fault is discretized using 798 elements for each layer.

We consider different configurations of the problem corresponding to different values of the permeabilities of the porous medium and the fault. In the first case we consider an homogeneous porous media with a permeability equal to $\Lambda = 10^{-17} \boldsymbol{I} m^2$. In this case we focus our attention on how the fault modifies the solution globally when we consider different values of its permeability. Figure 16 shows the initial

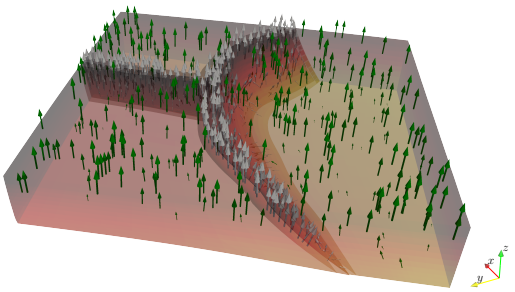
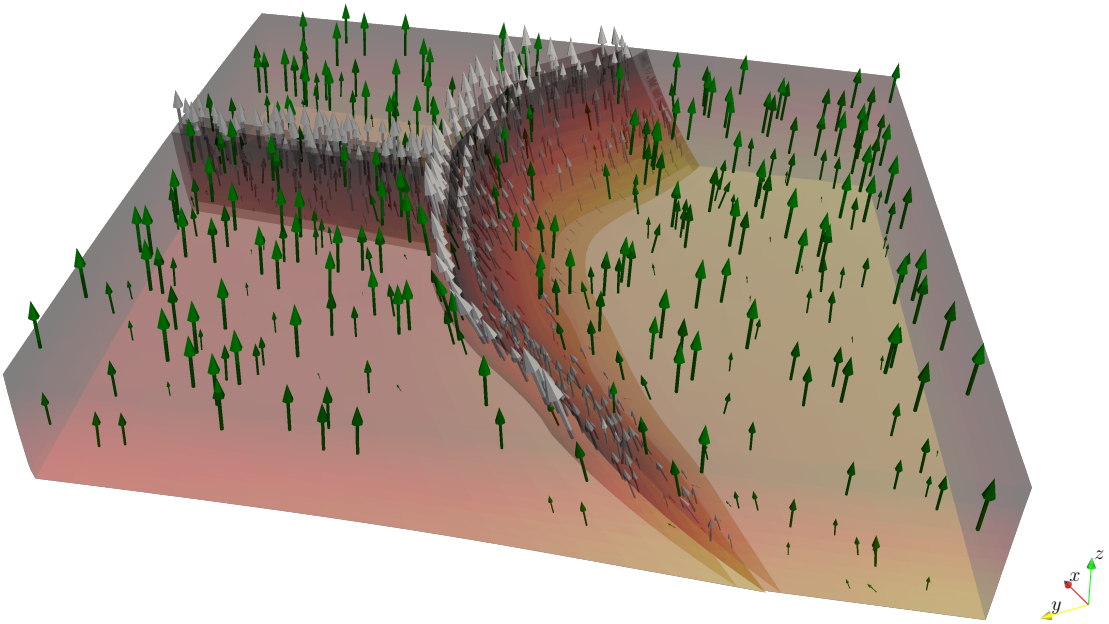


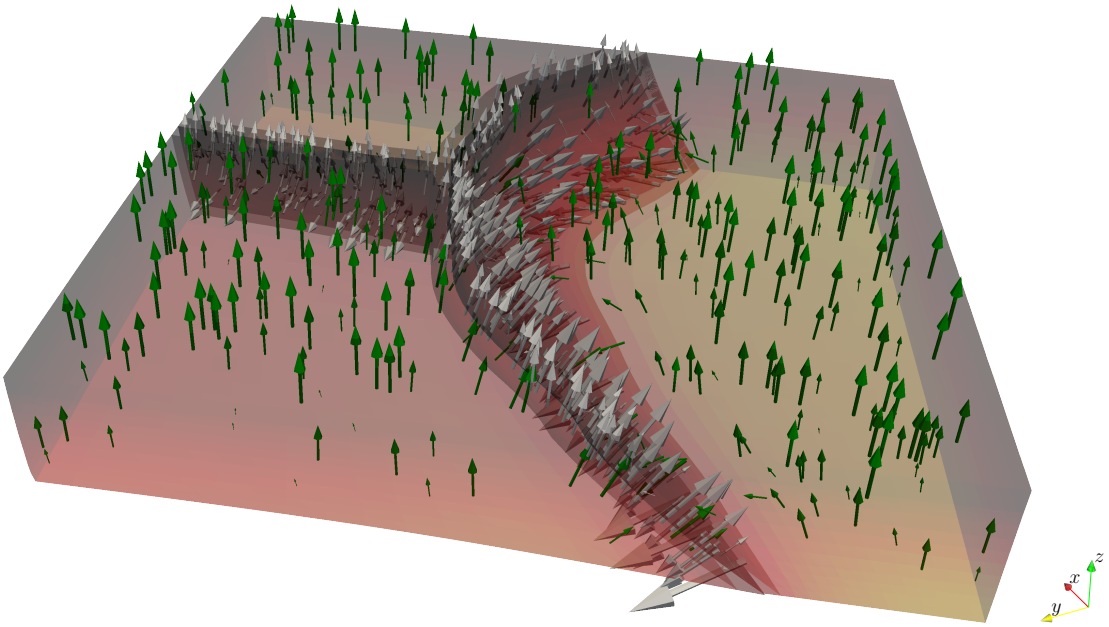
Figure 16: Initial solution for the homogeneous case.

solution. As in the two following figures we represent the Darcy solution with grey arrows in some of the cells close to the faults and with green arrows elsewhere. Since the permeability is constant we expect an almost linear solution for the pressure and a constant velocity. The solution respects the prevision.

We change now the permeability inside the fault considering two different scenarios, the fault is a barrier or the fault is a channel. In the first case we impose a fault permeability $\Lambda_f = 10^{-19} \boldsymbol{I} m^2$ while in the second case $\Lambda_f = 10^{-15} \boldsymbol{I} m^2$. In Figure 17 we present the solution for both cases. In Figure 17a the fault




(a) The fault behaves like a barrier.




(b) The fault behaves like a channel.

Figure 17: Solution for $t = 0.7My$ when the fault is a barrier or a channel for the flow.

clearly behaves like a barrier. Indeed we do not see any arrow that cross the fault and the Darcy velocity tends to follow the fault geometry. Not very far from the fault the flow is still vertical. The pressure has an almost linear shape from the bottom to the top of the domain. In the second case, reported in Figure 17b, the fault behaves like a conductive channel for the flow of the surrounding domain. We clearly see that the flow of the closer cells, represented by the grey arrows, are directed to the fault since it is easier for the flow to move inside the fault than to stay outside. Some of the green arrows close to the fault are pointing to the fault since the influence of the fault is stronger than in the previous case. The pressure is smaller for the cells close to the fault than in the previous case.

We change now the permeability of the porous medium to analyse the interaction between the heterogeneities and the fault. Considering Figure 15a, we impose as permeability in each of the black layer $\Lambda = 10^{-17}\boldsymbol{I}m^2$ while in each of the white layer $\Lambda = 10^{-15}\boldsymbol{I}m^2$. The black layers act as barriers while the latter are channels. The initial solution is represented in Figure 18. We can notice that far

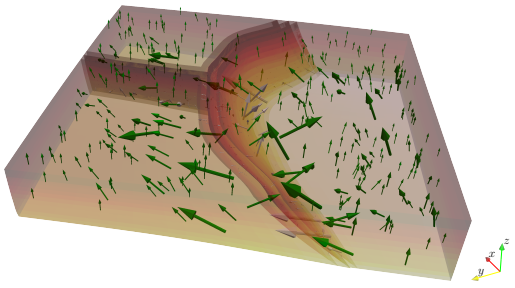


Figure 18: Initial solution for the heterogeneous case.

from the fault the flow is almost upward, while close to the fault and thanks to the non uniform strata deposition the solution is complicated and not easily predictable. Since the solution is much more complex than in the previous cases, as shown in Figure 18, we focus our attention only on the red cells represented in Figure 19. Thanks to the different layers the flow can pass from one permeable layer to the other following the fault or the less permeable

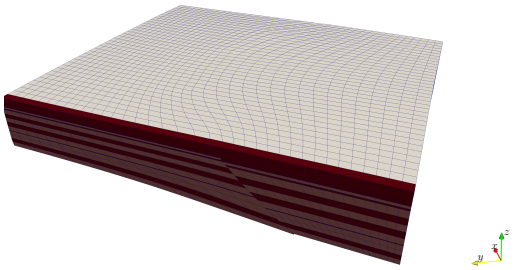
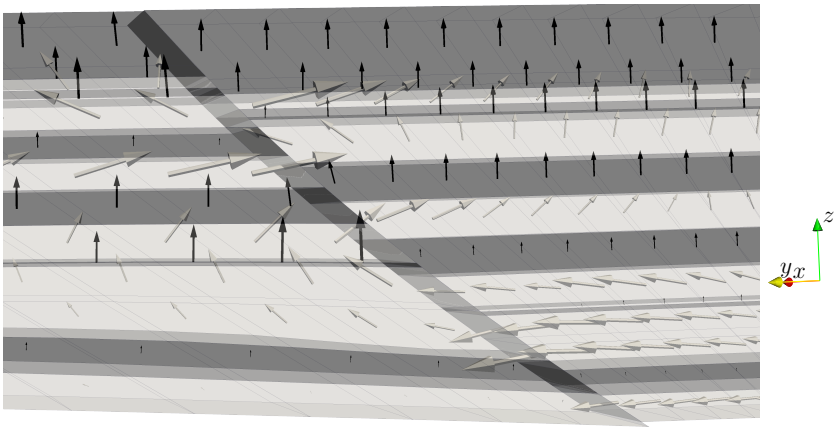
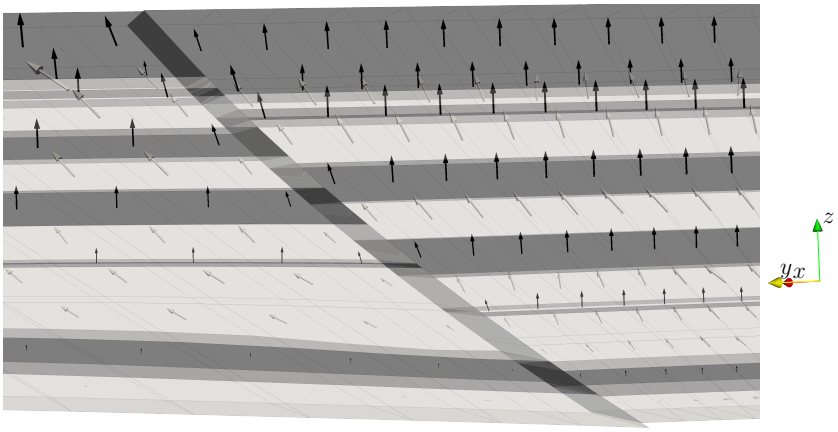


Figure 19: Set of cells where we focus our attention.

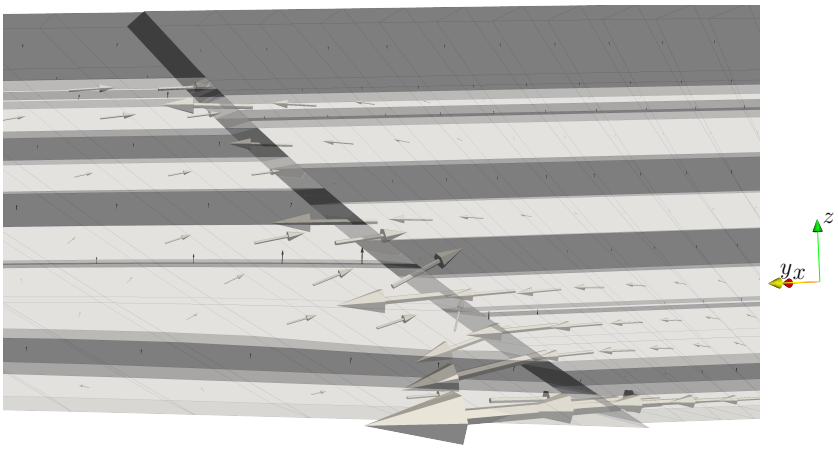
layers. We consider three different test cases changing the permeability in the fault. First of all we impose the permeability in the fault cells equal to that the neighbouring domain cell. In this case the fault behaves like the surrounding part of the domain. Figure 20a represents the Darcy velocity only in the selected cells. In the bottom part of the domain, thanks to the fault, the flow can pass through the latter and starts to move upward in the more permeable strata. In the middle of the domain, since the barrier in the left part of the domain is thinner than in the right part the flow is concentrated there. In the upper part of the domain the fluid moves from the left part to the right part and *vice versa*. In the second test case, represented in Figure 20b, we consider the fault as a barrier imposing a small permeability $\Lambda_f = 10^{-19}\boldsymbol{I}m^2$. We see that the arrows never cross the fault and the fluid moves only upward. Even considering the big black strata the flow avoids to pass through the fault. The Darcy velocity of the cells close to the fault is parallel to the fault surface. The last test considers a fault that behaves like a channel. In fact we impose $\Lambda_f = 10^{-13}\boldsymbol{I}m^2$ as the permeability in the fault. Figure 20c shows the Darcy velocity for $t = 0.7My$. The flow goes directly into the fault since the arrows are almost parallel to the layers and direct inward to the fault. Finally the Darcy flow is stronger close the fault and larger at the bottom of the domain then at the top. To conclude, in Figure 21 we present the global solution, Darcy velocity and pressure, for the neutral, barrier and for the channel. In these cases the solution is much more involved and difficult to analyse in




(a) The fault behaves like the surrounding medium.

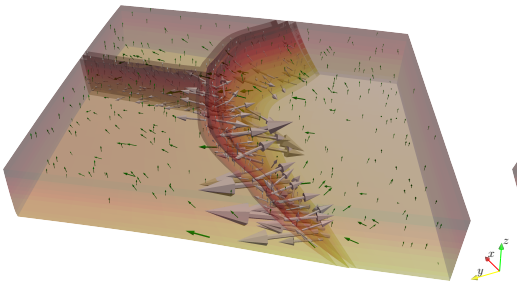



(b) The fault behaves like a barrier.

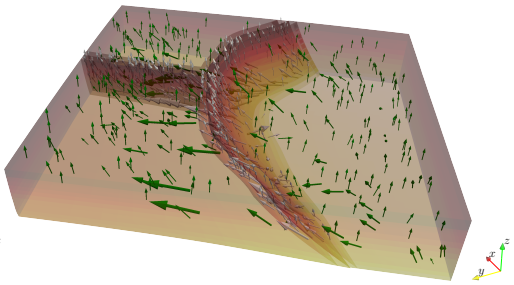



(c) The fault behaves like a channel.

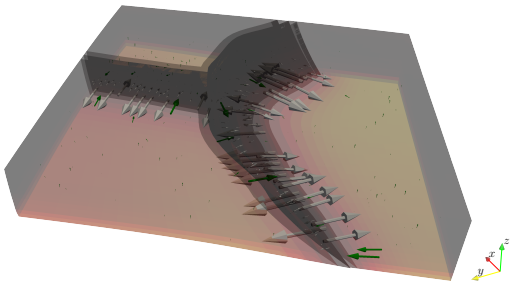
Figure 20: Solution for $t = 0.7My$ for different configurations of the fault. We use the same colour for cells and arrows according to the cell permeability where the arrow origin is located, like in Figure 15a. The scaling of the arrows in the three figures is different.



(a) The fault behaves like the surrounding medium.



(b) The fault behaves like a barrier.



(c) The fault behaves like a channel.

Figure 21: Solution for $t = 0.7My$ for different configurations of the fault.

| $\Omega$ | $\hat{\gamma}$ | ILU0 |
|---|---|---|
| homo. | barrier | 1 |
| homo. | channel | 3 |
| hete. | neutral | 3 |
| hete. | barrier | 2 |
| hete. | channel | 5 |

Table 1: Average of the number of iterations for different configurations.

detail. Anyway, especially for the barrier and the channel, the behaviour of the fault seams correct.

We have used an iterative scheme to solve the linear system. The algorithm chosen is the GMRES with tolerance on the stop criteria of $10^{-8}$ with ILU0 as preconditioner from PETSc library [6]. In Table 1 are reported the number of iterations for different configuration of the problem. We note that in all the case the preconditioner performs well.

# 6 Conclusion

In this paper we have presented a novel approximation of the double-layer reduced model to describe the fault flows in a complex porous medium. The reduced model is a reasonable approximation when the thickness of a fault is some order of magnitude smaller then its other sizes. Moreover the choice of the hybrid finite volume method allows us to handle, in a much robust and accurate way, different problem configurations. Particular attention is devoted to the analyses of the discrete equivalence that ease the implementation of the reduced model, for both the single-layer and double-layer model, avoiding to introduce the tangential operators and to approximate the coupling conditions. In the examples we have seen the correctness of the reduced model compared to a reference solution in several situations. Finally a real geometry with realistic data is presented to show the applicability to real problem. The solution behaves as expected and no evidence of serious problems is highlighted.

# 7 Acknowledgements

The authors wish to thank warmly Jean-Luc Rudkiewicz from IFP Energies nouvelles for building the mesh used in the realistic test case.

# A Appendix

## A.1 Nomenclature

We present the main nomenclature of this work. Some of the symbols are used only in one part of the domain, we use a subscript to indicate them. Some symbols for the numerical approximation can be found in Definition 1.

| | |
|---|---|
| $N$ | Dimension of the domain |
| $i$ | Index *s.t.* $i \in \{1, 2, f\}$ |
| $j$ | Index *s.t.* $j \in \{1, 2\}$ |
| $\Omega$ | Computational domain |
| $\Omega_f$ | Fault domain |
| $\Omega_{f_j}$ | Layer $j$ of $\Omega_f$ |
| $\hat{\gamma}$ | Fault centre |
| $d$ | Fault thickness |
| $\boldsymbol{n}$ | Normal to $\hat{\gamma}$ |
| $T_j$ | Normal thickness of $\Omega_{f_j}$ |
| $p$ | Pressure field |
| $\boldsymbol{u}$ | Darcy velocity |
| $\Lambda$ | Permeability matrix |
| $\lambda_{f,\boldsymbol{n}}$ | Normal fault permeability |
| $\lambda_{f,\boldsymbol{\tau}}$ | Tangential fault permeability |
| $q$ | Source term |
| $\boldsymbol{N}$ | Normal projection matrix |
| $\boldsymbol{T}$ | Tangential projection matrix |
| $\hat{p}$ | Reduced pressure |
| $\hat{\boldsymbol{u}}$ | Reduced Darcy velocity |
| $\hat{\lambda}$ | Reduced tangential permeability |
| $\lambda_{\hat{\gamma}}$ | Reduced normal permeability |
| $\hat{q}$ | Reduced source term |
| $\hat{u}_{\boldsymbol{n}}$ | Interface Darcy velocity normal to $\hat{\gamma}$ |
| $\nabla_{\boldsymbol{\tau}}$ | Tangential gradient to $\hat{\gamma}$ |
| $\nabla_{\boldsymbol{\tau}}\cdot$ | Tangential divergence to $\hat{\gamma}$ |
| $\nabla_{\mathcal{D}}$ | Discrete gradient |
| $\nabla_K$ | Discrete cell gradient |
| $R_{K,\sigma}$ | Stabilization term for $\nabla_{\mathcal{D}}$ |
| $\alpha$ | Stabilization parameter |
| $\hat{\alpha}$ | Reduced stabilization parameter |
| $[\![\cdot]\!]_\gamma$ | Jump operator across $\gamma$ |
| $\{\!\{\cdot\}\!\}_\gamma$ | Mean operator across $\gamma$ |

## A.2 The hybrid finite volume scheme

The HFV scheme is a cell-centred finite volume scheme, with unknowns on each edge and on each cell of the computational grid, that gives an approximation of conductive fluxes on non-conforming grids. Its principle, using a finite volume philosophy, is briefly recalled in this section. A more detailed presentation can be found in [16, 15]. The model problem is: find the unknown $p$ such that

$$\begin{aligned} -\nabla\cdot\Lambda\nabla p &= q \quad \text{in } \Omega \\ p &= 0 \quad \text{on } \partial\Omega \end{aligned} \tag{33}$$

We consider the computational grid, approximation of $\Omega$, defined as in Definition 1. Integrating (33) over each control volume $K \in \mathcal{M}$, gives the following

$$\sum_{\sigma\in\mathcal{E}_K}\int_\sigma \Lambda\nabla p\cdot\boldsymbol{n}_{K,\sigma}\mathrm{d}\sigma = \int_K q\mathrm{d}x \quad \forall K\in\mathcal{M}.$$

The flux $\int_\sigma \Lambda\nabla p\cdot\boldsymbol{n}_{K,\sigma}\mathrm{d}\sigma$ on each mesh edge $\sigma\in\mathcal{E}_K$ is approximated through a numerical flux function $F_{K,\sigma}(p)$ which depends only on the local unknowns related to $K$ and $\mathcal{E}_K$. The discrete approximation of (33) is given by

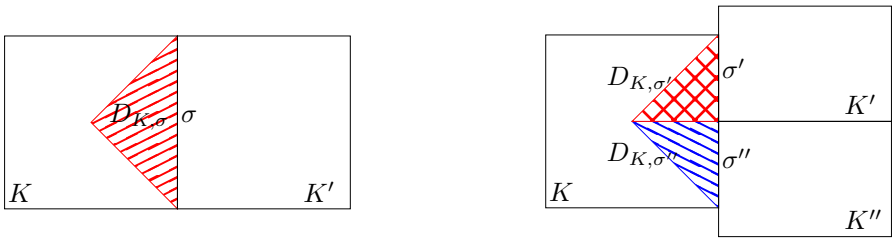
$$\sum_{\sigma\in\mathcal{E}_K} F_{K,\sigma}(p) = \int_K q\mathrm{d}x \quad \forall K\in\mathcal{M}. \tag{34}$$

Since the previous system is defined cell-wise, we require the continuity of the flux on all the interior edges, imposing

$$F_{K,\sigma}(p) + F_{L,\sigma}(p) = 0 \quad \forall\sigma\in\mathcal{E}_{\text{int}} \tag{35}$$

with $\mathcal{M}_\sigma = \{K, L\}$. We express now the equations (34) and (35), introducing the test functions $v$ constant for each cell $K\in\mathcal{M}$ as

$$\langle p, v\rangle_F = \sum_{K\in\mathcal{M}} v_K\int_K qv_K\mathrm{d}x,$$




(a) Matching cells

(b) Non-matching cells

Figure 22: Representation of the subdivision in cones for a matching pair of cells and for non-matching cells.

where the bilinear form is defined as

$$\langle p, v\rangle_F := \sum_{K\in\mathcal{M}}\sum_{\sigma\in\mathcal{E}_K} F_{K,\sigma}(p)\,(v_K - v_\sigma)\,.$$

The HFV scheme is based on a suitable choice of the discrete gradient $\nabla_{\mathcal{D}}\, p$, approximation of $\nabla p$, such that the following relation holds true

$$\langle p, v\rangle_F = \sum_{K\in\mathcal{M}} (\Lambda\nabla_{\mathcal{D}}\, p, \nabla_{\mathcal{D}}\, v)_K\,.$$

The discrete gradient is chosen such that the bilinear form is coercive, the matrix of the associated linear system is symmetric definite positive and fulfil a suitable convergence property. Following [16, 15] we introduce the cell gradient

$$\nabla_K p := \frac{1}{|K|}\sum_{\sigma\in\mathcal{E}_K} |\sigma|\,(p_\sigma - p_K)\,\boldsymbol{n}_{K,\sigma}$$

and a cone stabilization term, zero for linear solutions, which gives the definiteness property for the discrete bilinear form:

$$R_{K,\sigma}p := \frac{\beta}{d_{K,\sigma}}\left[p_\sigma - p_K - \nabla_K p\cdot(\boldsymbol{x}_\sigma - \boldsymbol{x}_K)\right],$$

with $\beta = \alpha\sqrt{N}$ and $\alpha$ a stabilization parameter which can vary between each cell. If $R_{K,\sigma}$ is not considered, the cell unknowns are not uniquely defined and the corresponding linear system is singular. Finally the discrete gradient $\nabla_{\mathcal{D}}\, p$ is defined for each cone $D_{K,\sigma}\subset K$ as

$$\nabla_{\mathcal{D}}\, p|_{D_{K,\sigma}} := \nabla_K p + R_{K,\sigma}p\boldsymbol{n}_{K,\sigma}.$$

It is shown that then, the bilinear form writes

$$\langle p, v\rangle_F = \sum_{K\in\mathcal{M}} |K|\,\Lambda_K\nabla_K p\cdot\nabla_K v + \tag{36}$$
$$+\sum_{\sigma\in\mathcal{E}_K}\alpha^2\frac{|\sigma|\,d_{K,\sigma}}{d}R_{K,\sigma}pR_{K,\sigma}v\boldsymbol{n}_{K,\sigma}\cdot\Lambda_K\boldsymbol{n}_{K,\sigma}$$

It can be derived also a closed form for the discrete flux $F_{K,\sigma}$, which can be expressed as

$$F_{K,\sigma}(p) = \sum_{\sigma'\in\mathcal{E}_K} A_K^{\sigma\sigma'}\,(p_K - p_{\sigma'})\,,$$

with $(A_K^{\sigma\sigma'})_{\sigma\sigma'\in\mathcal{E}_K}$ a local symmetric and positive matrix. Its expression can be found in [16].

**Remark 3.** *The extension of the HFV scheme to a non-conforming grid is natural. Instead of considering edges of the mesh, we consider sub-edges, i.e. computed intersecting edges of different cells, and then for the construction of the discrete gradient the cones are built based on the sub-edges. An example is reported in Figure 22.*

Finally the following lemma presents the equivalence between the HFV scheme and the classical TPFA scheme.

**Lemma 1** (Lemma 2.1 [16])**.** *If the discretization of $\Omega$ satisfy the superadmissible condition*

$$\boldsymbol{n}_{K,\sigma} = (\boldsymbol{x}_\sigma - \boldsymbol{x}_K)/d_{K,\sigma}\quad \forall K\in\mathcal{M}, \forall\sigma\in\mathcal{E}_K$$

*and $\Lambda(x) = \lambda(x)\boldsymbol{I}$, with $\lambda$ piece-wise constant on $\mathcal{M}$ and choosing for each edge $\sigma\in\mathcal{E}_{\text{int}}$*

$$\boldsymbol{x}_\sigma = \frac{d_{K,\sigma}\boldsymbol{x}_L + d_{L,\sigma}\boldsymbol{x}_K}{d_{K,\sigma}+d_{L,\sigma}}\ \text{ with } \mathcal{M}_\sigma = \{K, L\}$$

*then the HFV scheme is equivalent to a two-point scheme. The scheme is defined as follow*

$$\sum_{\sigma\in\mathcal{E}_K} F_{K,\sigma}(p) = \int_K q\mathrm{d}x$$

$$F_{K,\sigma} = \begin{cases} \dfrac{\lambda_\alpha\,|\sigma|}{d_{K,\sigma}+d_{L,\sigma}}(p_K - p_L) & \text{if } \sigma\in\mathcal{E}_{\text{int}} \\ \dfrac{\lambda_K\,|\sigma|}{d_{K,\sigma}}p_K & \text{if } \sigma\in\mathcal{E}_{\text{ext}} \end{cases}$$

*with* $\mathcal{M}_\sigma = \{K, L\}$ *and*

$$\lambda_\alpha = \frac{\lambda_K\lambda_L(d_{K,\sigma}+d_{L,\sigma})}{\lambda_K d_{L,\sigma}+\lambda_L d_{K,\sigma}}.$$

**Remark 4.** *An extension, presented in [13], of the HFV scheme considers a stabilization parameter that is no more a scalar but a matrix. The stabilization term in* (36) *becomes*

$$\sum_{K\in\mathcal{M}}\sum_{\sigma,\sigma'\in\mathcal{E}_K} B_{K,\sigma,\sigma'}S_{K,\sigma}pS_{K,\sigma'}v,$$

*with* $(B_{K,\sigma,\sigma'})_{\sigma,\sigma'\in\mathcal{E}_K}$ *a symmetric and positive matrix for the cell* $K\in\mathcal{M}$ *and*

$$S_{K,\sigma}p := p_\sigma - p_K - \nabla_K p\cdot(\boldsymbol{x}_\sigma - \boldsymbol{x}_K)\,.$$

# References


[1] Pierre M. Adler and Jean-François Thovert. *Fractures and fracture networks*. Springer, 1999.

[2] Pierre M. Adler, Jean-François Thovert, and Valeri V. Mourzenko. *Fractured porous media*. Oxford University Press, 2012.

[3] Clarisse Alboin, Jérôme Jaffré, Jean E. Roberts, Xuewen Wang, and Christophe Serres. *Domain decomposition for some transmission problems in flow in porous media*, volume 552 of *Lecture Notes in Phys.*, pages 22–34. Springer, Berlin, 2000.

[4] Philippe Angot, Franck Boyer, and Florence Hubert. Asymptotic and numerical modelling of flows in fractured porous media. *M2AN Math. Model. Numer. Anal.*, 43(2):239–275, 2009.

[5] R. G. Baca, R. C. Arnett, and D. W. Langford. Modelling fluid flow in fractured-porous rock masses by finite-element techniques. *International Journal for Numerical Methods in Fluids*, 4(4):337–348, 1984.

[6] Satish Balay, Jed Brown, Kris Buschelman, Victor Eijkhout, William D. Gropp, Dinesh Kaushik, Matthew G. Knepley, Lois Curfman McInnes, Barry F. Smith, and Hong Zhang. PETSc users manual. Technical Report ANL-95/11 - Revision 3.4, Argonne National Laboratory, 2013.

[7] Jacob Bear, Chin-Fu Tsang, and G de Marsily. *Flow and contaminant transport in fractured rock*. Academic Press, San Diego, 1993.

[8] Brian Berkowitz. Characterizing flow and transport in fractured geological media: A review. *Advances in Water Resources*, 25(8-12):861–884, 2002.

[9] Denis Biryukov and Fikri J. Kuchuk. Transient pressure behavior of reservoirs with discrete conductive faults and fractures. *Transport in Porous Media*, 95(1):239–268, 2012.

[10] Kostantin Brenner, Mayya Groza, C. Guichard, and Roland Masson. Vertex approximate gradient scheme for hybrid dimensional two-phase darcy flows in fractured porous media. *ESAIM: Mathematical Modelling and Numerical Analysis*, 49(2):303–330, 2015.

[11] Franco Brezzi and Michel Fortin. *Mixed and Hybrid Finite Element Methods*, volume 15 of *Computational Mathematics*. Springer Verlag, Berlin, 1991.

[12] Carlo D'Angelo and Anna Scotti. A mixed finite element method for Darcy flow in fractured porous media with non-matching grids. *Mathematical Modelling and Numerical Analysis*, 46(02):465–489, 2012.

[13] Jérôme Droniou, Robert Eymard, Thierry Gallouët, and Raphaèle Herbin. A unified approach to mimetic finite difference,

hybird finite volume and mixed finite volume methods. *Mathematical Models and Methods in Applied Sciences*, 20(02):265–295, 2010.

[14] Alexandre Ern and Jean-Luc Guermond. *Theory and practice of finite elements*. Applied mathematical sciences. Springer, 2004.

[15] Robert Eymard, Thierry Gallouët, and Raphaèle Herbin. A new finite volume scheme for anisotropic diffusion problems on general grids: convergence analysis. *Comptes Rendus Mathematique*, 344(6):403–406, 2007.

[16] Robert Eymard, Thierry Gallout, and Raphaèle Herbin. Discretization of heterogeneous and anisotropic diffusion problems on general nonconforming meshes sushi: a scheme using stabilization and hybrid interfaces. *IMA Journal of Numerical Analysis*, 30(4):1009–1043, 2010.

[17] Isabelle Faille, Eric Flauraud, Frédéric Nataf, Sylvie Pégaz-Fiornet, Frédéric Schneider, and Françoise Willien. A new fault model in geological basin modelling. Application of finite volume scheme and domain decomposition methods. In *Finite volumes for complex applications, III (Porquerolles, 2002)*, pages 529–536. Hermes Sci. Publ., Paris, 2002.

[18] Isabelle Faille, Frédéric Nataf, Laurent Saas, and Françoise Willien. Finite Volume Methods on Non-Matching Grids with Arbitrary Interface Conditions and Highly Heterogeneous Media. In TimothyJ. Barth, Michael Griebel, DavidE. Keyes, RistoM. Nieminen, Dirk Roose, Tamar Schlick, Ralf Kornhuber, Ronald Hoppe, Jacques Priaux, Olivier Pironneau, Olof Widlund, and Jinchao Xu, editors, *Domain Decomposition Methods in Science and Engineering*, volume 40 of *Lecture Notes in Computational Science and Engineering*, pages 243–250. Springer Berlin Heidelberg, 2005.

[19] Luca Formaggia, Alessio Fumagalli, Anna Scotti, and Paolo Ruffo. A reduced model for Darcy's problem in networks of fractures. *ESAIM: Mathematical Modelling and Numerical Analysis*, 48:1089–1116, 7 2014.

[20] Najla Frih, Vincent Martin, Jean E. Roberts, and Ai Saâda. Modeling fractures as interfaces with nonmatching grids. *Computational Geosciences*, 16(4):1043–1060, 2012.

[21] Najla Frih, Jean E. Roberts, and Ali Saada. Modeling fractures as interfaces: a model for Forchheimer fractures. *Computers and Geosciences*, 12(1):91–104, 2008.

[22] Alessio Fumagalli and Anna Scotti. A numerical method for two-phase flow in fractured porous media with non-matching grids. *Advances in Water Resources*, 62, Part C(0):454–464, 2013. Computational Methods in Geologic CO2 Sequestration.

[23] Alessio Fumagalli and Anna Scotti. An efficient xfem approximation of darcy flow in arbitrarly fractured porous media. *Oil and Gas Sciences and Technologies - Revue d'IFP Energies Nouvelles*, 69(4):555–564, April 2014.

[24] Håkon Hægland, Anongnart Assteerawatt, Helge K. Dahle, Geir Terje Eigestad, and Rainer Helmig. Comparison of cell- and vertex-centered discretization methods for flow in a two-dimensional discrete-fracture-matrix system. *Advances in Water Resources*, 32(12):1740–1755, 2009.

[25] Hussein Hoteit and Abbas Firoozabadi. Multicomponent fluid flow by discontinuous galerkin and mixed methods in unfractured and fractured media. *Water Resources Research*, 41(11), 2005.

[26] Hussein Hoteit and Abbas Firoozabadi. An efficient numerical model for incompressible two-phase flow in fractured media. *Advances in Water Resources*, 31(6):891–905, June 2008.

[27] Hao Huang, Ted A. Long, Jing Wan, and William P. Brown. On the use of enriched finite element method to model subsurface features in porous media flow problems. *Computational Geosciences*, 15(4):721–736, 2011.

[28] Jérôme Jaffré, M. Mnejja, and Jean E. Roberts. A discrete fracture model for two-phase flow with matrix-fracture interaction. *Procedia Computer Science*, 4:967–973, 2011.

[29] Mohammad Karimi-Fard, Luis J. Durlofsky, and K. Aziz. An Efficient Discrete-Fracture Model Applicable for General-Purpose Reservoir Simulators. *SPE Journal*, 9(2):227–236, 2004.

[30] Mohammad Karimi-Fard and Abbas Firoozabadi. Numerical simulation of water injection in fractured media using the discrete-fracture model and the galerkin method. *SPE Reservoir Evaluation & Engineering*, 6(02):117–126, 2003.

[31] Peter Knabner and Jean E. Roberts. Mathematical analysis of a discrete fracture model coupling darcy flow in the matrix with darcy-forchheimer flow in the fracture. *ESAIM: Mathematical Modelling and Numerical Analysis*, 48:1451–1472, 9 2014.

[32] Vincent Martin, Jérôme Jaffré, and Jean E. Roberts. Modeling fractures and barriers as interfaces for flow in porous media. *SIAM J. Sci. Comput.*, 26(5):1667–1691, 2005.

[33] Jorge E. P. Monteguado and Abbas Firoozabadi. Control-volume method for numerical simulation of two-phase immiscible flow in two- and three-dimensional discrete-fractured media. *Water Resources Research*, 40(7):n/a–n/a, 2004.

[34] Fernando Morales and Ralph E. Showalter. The narrow fracture approximation by channeled flow. *Journal of Mathematical Analysis and Applications*, 365(1):320–331, 2010.

[35] Fernando Morales and Ralph E. Showalter. Interface approximation of darcy flow in a narrow channel. *Mathematical Methods in the Applied Sciences*, 35(2):182–195, 2012.

[36] Alfio Quarteroni and Alberto Valli. *Numerical approximation of partial differential equations*, volume 23 of *Springer Series in Computational Mathematics*. Springer-Verlag, Berlin, 1994.

[37] Volker Reichenberger, Hartmut Jakobs, Peter Bastian, and Rainer Helmig. A mixed-dimensional finite volume method for two-phase flow in fractured porous media. *Advances in Water Resources*, 29(7):1020–1036, 2006.

[38] Jean E. Roberts and Jean-Marie Thomas. Mixed and hybrid methods. In *Handbook of numerical analysis, Vol. II*, Handb. Numer. Anal., II, pages 523–639. North-Holland, Amsterdam, 1991.

[39] Xavier Tunc, Isabelle Faille, Thierry Gallouët, Marie Christine Cacas, and Pascal Havé. A model for conductive faults with non-matching grids. *Computational Geosciences*, 16:277–296, 2012.